Journal of Medicinal Chemistry

Article

Discovery of Potent and Selective Inhibitors of Phosphodiesterase 1 for the Treatment of Cognitive Impairment Associated with Neurodegenerative and Neuropsychiatric Diseases

Peng Li, Hailin Zheng, Jun Zhao, Lei Zhang, Wei Yao, Hongwen Zhu, J. David Beard, Koh Ida, Weston Lane, Gyorgy Snell, Satoshi Sogabe, Charles J. Heyser, Gretchen L. Snyder, Joseph P. Hendrick, Kimberly E. Vanover, Robert E. Davis, and Lawrence P Wennogle

J. Med. Chem., **Just Accepted Manuscript** • DOI: 10.1021/acs.jmedchem.5b01751 • Publication Date (Web): 20 Jan 2016

Just Accepted

ACS Publications

Journal of Medicinal Chemistry is published by the American Chemical Society. 1155 Sixteenth Street N.W., Washington, DC 20036

Discovery of Potent and Selective Inhibitors of Phosphodiesterase 1 for the Treatment of Cognitive Impairment Associated with Neurodegenerative and Neuropsychiatric Diseases

Peng Li,[*,†] Hailin Zheng,[†] Jun Zhao,[†,€] Lei Zhang,[†] Wei Yao,[†] Hongwen Zhu,[†,£] J. David Beard,[†] Koh Ida,[¶] Weston Lane,[‡] Gyorgy Snell,[‡] Satoshi Sogabe,[¶] Charles J. Heyser,[§] Gretchen L. Snyder,[†] Joseph P. Hendrick,[†] Kimberly E. Vanover,[†] Robert E. Davis[†] and Lawrence P. Wennogle[†]

[†]Intra-Cellular Therapies, Inc., 430 East 29th Street, Suite 900, New York, New York, 10016, United States

[‡]Department of Structural Biology, Takeda California, Inc., 10410 Science Center Dr., San Diego, California 92121, United States

[¶]Pharmaceutical Research Division, Takeda Pharmaceutical Company, Ltd., 26-1, Muraoka-Higashi 2-chome, Fujisawa, Kanagawa 251-8555, Japan

[§]Department of Neurosciences, University of California, San Diego, 9500 Gilman Dr. #0608, La Jolla, California, 92093, United States

---

[*] Author to whom correspondence should be addressed

Peng Li, Ph.D.
Vice President, Medicinal Chemistry
Intra-Cellular Therapies, Inc.
430 East 29th Street, Suite 900
New York, NY 10016
Phone: 646-440-9388
Email: pli@intracellulartherapies.com

ABSTRACT

A diverse set of 3-aminopyrazolo[3,4-*d*]pyrimidinones was designed and synthesized. The structure-activity relationships of these polycyclic compounds as phosphodiesterase 1 (PDE1) inhibitors were studied along with their physicochemical and pharmacokinetic properties. Systematic optimizations of this novel scaffold culminated in the identification of a clinical candidate, (6a*R*,9a*S*)-2-(4-(6-fluoropyridin-2-yl)benzyl)-5-methyl-3-(phenylamino)-5,6a,7,8,9,9a-hexahydrocyclopenta[4,5]imidazo[1,2-*a*]pyrazolo[4,3-*e*]pyrimidin-4-(2*H*)-one phosphate (ITI-214), which exhibited picomolar inhibitory potency for PDE1, demonstrated excellent selectivity against all other PDE families, and showed good efficacy *in vivo*. Currently, this investigational new drug is in Phase I clinical development and being considered for the treatment of several indications including cognitive deficits associated with schizophrenia and Alzheimer's disease, movement disorders, attention deficit and hyperactivity disorders, and other CNS and non-CNS disorders.

INTRODUCTION

3',5'-Cyclic adenosine monophosphate (cAMP) and 3',5'-cyclic guanosine monophosphate (cGMP, **1**) play important roles in signal transduction and synaptic transmission.[1] Cyclic nucleotide phosphodiesterases (PDEs) degrade cAMP and cGMP by hydrolysis of 3'-phosphodiester bonds, and consequently regulate intracellular levels of these ubiquitous second messengers.[2] To date, 11 different PDE families (PDE1 to PDE11) have been identified, encoded by 21 genes.[3] Unique among the PDEs, the enzymes of the PDE1 family are tightly regulated by intracellular calcium and calmodulin levels.[4,5] Rises in intracellular calcium lead to increased PDE1 activity and result in increased cyclic nucleotide degradation. PDE1 enzymes are dual cyclic nucleotide phosphodiesterases that can accommodate and hydrolyze both cAMP and cGMP.[6] The ability of PDE1 to hydrolyze both cAMP and cGMP allows these enzymes to dynamically influence signaling in multiple excitatory cell systems.

PDE1 exists as three isoforms (PDE1A, 1B and 1C), derived from three distinct genes. Each of these isoforms has multiple splice variants.[5] These isoforms/splice variants appear to be distributed in a cell type-specific manner in the brain and other tissues. For example, in the brain the predominant expression of PDE1A is in the cortex and neostriatum, PDE1B is in the neostriatum, prefrontal cortex, hippocampus and olfactory tubercle and PDE1C is more ubiquitously expressed.[7] The cell type specific expression as well as regulation by intracellular calcium and calmodulin, and regionally specific localizations of the PDE1 isoforms place these enzymes in a position to influence phasic, but not tonic signaling from diverse neurotransmitter systems. These systems include those utilizing dopamine, acetylcholine, glutamate and certain peptidergic systems.[7] As one example, PDE1B is co-localized with dopamine D1 receptors (D1R), which initiate signal transduction via production of cAMP. Both PDE1B and D1R are abundantly expressed in the prefrontal cortex, a brain region that governs working memory function.[7–9] Modulation of dopamine function through D1 receptors has been shown to alter certain mnemonic processes.[10] Insufficient D1R-mediated signaling in the prefrontal cortex has been shown to impair cognitive function in both preclinical and clinical studies.[11] As D1 receptors signal through modulation of adenylate cyclase and production of cAMP, inhibition of PDE1 will amplify dopaminergic neurotransmission downstream of these receptors. Increased D1R-mediated signaling would be expected to ameliorate cognitive deficits associated with schizophrenia,[12,13] as well as other central nervous system (CNS) and non-CNS disorders. However, the foregoing does not preclude the possibility that PDE1 inhibition may also modulate other neurotransmitter systems that signal through either cAMP or cGMP systems. Changes in these neurotransmitter systems are known to influence cognitive function and include dopaminergic, muscarinic, glutamatergic and nitric oxide systems. Thus, by uniquely preventing degradation of both cAMP and cGMP signaling, PDE1 inhibition is likely to improve cognitive function in a variety of neurodegenerative and neuropsychiatric diseases, including schizophrenia, Parkinson's disease and dementia.[14]

The role of PDE1 in excitatory cellular systems compelled us to design PDE1 specific inhibitors for the treatment of cognitive dysfunction. Since the catalytic domains of all PDE enzymes share a high de-

gree of sequence homology, this was an ambitious endeavor. The key interactions of substrates at the catalytic sites of these PDE enzymes include an important hydrogen bond with a conserved active-site glutamine and a hydrophobic clamp that sandwiches the purine-like core of the cAMP or cGMP, as confirmed by X-ray crystallography.[15–17] Various PDE1 inhibitors with different heterocyclic systems mimicking the structure of guanine have been documented.[18,19] However, most of the known PDE1 inhibitors in the public domain show inhibitory activity to other PDE enzymes in addition to PDE1. Achieving high selectivity between enzymes of the PDE superfamily can be a challenging task, yet necessary in order to develop PDE drug candidates with good safety profiles. In particular, drug candidates need to avoid PDE6 activity to minimize effects on vision.[20]

In an effort to develop potent and selective PDE1 inhibitors for the treatment of symptoms associated with neuropsychiatric and neurodegenerative diseases, we analyzed the published PDE inhibitors with different chemical scaffolds and found the pyrazolo[3,4-*d*]pyrimidinones reported by Xia and coworkers could be a good starting point for design of new PDE1 inhibitors.[19] These compounds were developed as PDE1 and PDE5 dual inhibitors with nanomolar to micromolar inhibitory activities. According to the published X-ray structures of PDE enzymes complexed with cGMP and various PDE inhibitors mimicking guanine,[15–17] the *N*-7 nitrogen in the purine ring of guanine usually forms a hydrogen bond with an adjacent amino acid residue located in the catalytic site. For the pyrazolo[3,4-*d*]pyrimidinone series of compounds, the shift of the nitrogen from position 3 to position 2 of the pyrazole ring could disrupt the hydrogen bond network. To re-establish the hydrogen bond mentioned above, we designed the polycyclic 3-aminopyrazolo[3,4-*d*]pyrimidinone scaffold **2** with the intention to form the important hydrogen bond through the amino group substitution at carbon-3 of the pyrazole ring (Figure 1). By the combined use of ligand-based and structure-based drug design processes, we have designed and developed multiple novel scaffolds as PDE1 inhibitors. In this paper, we will focus our discussion on the development and structure-activity relationships (SAR) of the polycyclic 3-aminopyrazolo[3,4-*d*]pyrimidinone scaffold **2** as novel PDE1 inhibitors. This work led to the discovery of (6a*R*,9a*S*)-2-(4-(6-fluoropyridin-2-yl)benzyl)-5-methyl-3-(phenylamino)-5,6a,7,8,9,9a-

hexahydrocyclopenta[4,5]-imidazo[1,2-*a*]pyrazolo[4,3-*e*]pyrimidin-4-(2*H*)-one phosphate (**3**, ITI-214), which is a picomolar PDE1 inhibitor with excellent selectivity against other PDE family members and against a panel of enzymes, receptors, transporters and ion channels. Currently, compound **3** is in human clinical trials.

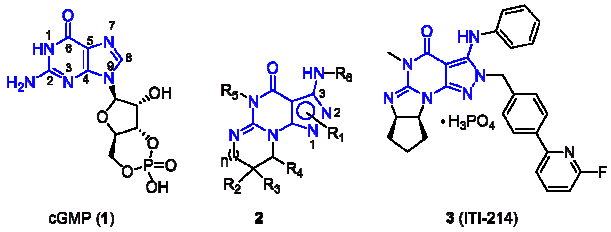

Figure 1. Structures of cGMP (1), 3-amino-pyrazolo[3,4-*d*]pyrimidine scaffold (2) and compound 3.

CHEMISTRY

To efficiently synthesize a diverse set of polycyclic pyrazolo[3,4-*d*]pyrimidinone compounds for SAR studies, several synthetic methods have been developed as illustrated in Schemes 1–3. The synthetic route exemplified in Scheme 1 was employed to conveniently explore the SAR of the left lower moiety of this series of compounds with variations of substituents (R_2–R_4), ring size (n) and stereochemistry. Commercially available 6-chloro-3-methyluracil was first protected with a para-methoxybenzyl (PMB) group, followed by chlorine displacement with hydrazine hydrate to give compound **5**. Treatment of **5** with phenyl isothiocyanate using a procedure developed based on a reported method allowed us to construct the pyrazolo[3,4-*d*]pyrimidinone ring system and introduce a phenylamino group at position 3 in one step.[21] The obtained compound **6** was then reacted with a para-substituted benzyl halide to give *N*2-substituted **7** as the major product along with a small amount of *N*1-substituted isomer, which can be readily separated by column chromatography. After the removal of the PMB protective group with trifluoromethanesulfonic acid (TfOH) and trifluoroacetic acid (TFA), the resulting compound **8** was chlo-

rinated with phosphorus oxychloride to furnish the key intermediate **9**. Reaction of **9** with various amino alcohols $HOCHR_4CR_2R_3(CH_2)_nNH_2$ followed by ring-closure with thionyl chloride afforded the final products **19**–**23**, **25**–**29**, **38** and **66**, as listed in Tables 1 and 4. Compound **24** was synthesized by debenzylation of **27** with boron trichloride.

To expedite the SAR development of compounds with variations of substituents at position *N*1 or *N*2 of the pyrazole ring, another synthetic route was developed, as illustrated in Scheme 2. Intermediate **6** was deprotected with TfOH and TFA, followed by chlorination with phosphorus oxychloride to afford **10**. Amination of **10** with (1*R*,2*R*)-2-aminocyclopentanol upon heating produced **11**, which was treated with thionyl chloride to afford the tetracyclic intermediate **12**. For rapidly generating analogs, the sidechain R was introduced in the last step of the synthesis by reacting **12** with a halide RX. Thus, *N*1-substituted compounds **30**–**36**, **39**, **44** and **46** were obtained as the major products. *N*2-substituted isomers **37**, **40**–**43**, **45**, **47** and **67**–**69** can also be prepared using this method.

The third synthetic route was developed to rapidly explore the SAR of the substituents at position 3 of the pyrazole ring, as illustrated in Scheme 3. Intermediate **5** was treated with $POCl_3$ and DMF to afford **13**. Benzylation of **13** with 2-(4-(chloromethyl)phenyl)-6-fluoropyridine gives exclusively the *N*2-substituted compound **14**, which upon treatment with TfOH and TFA furnished **15**. Compound **16** was synthesized from **15** by BOP-mediated direct amination.[22] The subsequent stereoselective ring-closure was achieved by treating **16** with *N,N*-dimethylchloro-sulfitemethaniminium chloride, *in situ* generated from thionyl chloride and DMF,[23] to afford tetracyclic compound **17**. Chlorination of **17** with Lithium bis(trimethylsilyl)amide (LiHMDS) and hexachloroethane produced the key intermediate **18**, which enables us to efficiently introduce various substituents into position 3 in the final step of the synthesis. For instance, 3-alkylamino and 3-benzylamino substituted compounds **49**–**57** and **59** can be conveniently synthesized by reacting **18** with the corresponding amines at elevated temperature. Reaction of **18** with 4-methoxybenzyl amine followed by PMB deprotection with TfOH and TFA yielded compound **48**. 3-Phenylamino substituted compound **3** was prepared from **18** in good yields by a palladium-catalyzed

cross-coupling reaction using tris(dibenzylideneacetone)dipalladium ($Pd_2(dba)_3$) as a catalyst and Xantphos as a ligand. Compounds **58** and **71** were synthesized by reacting **18** with pyridin-4-amine and 4-fluorobenzenamine, respectively, using LiHMDS as a strong base. Aryloxy-substituted **72** and **73** were produced by treating **18** with the corresponding aryl alcohols and potassium carbonate at 150 °C. Methylation of **3** with methyl iodide and cesium carbonate furnished **60**. Compound **74** with a phenylthio group at position 3 was prepared by treating **17** with LiHMDS and phenyl disulfide. Synthesis of 3-benzyl substituted **75** and **76** were accomplished by Pd-catalyzed Suzuki coupling of **18** with borate intermediates, which were produced *in situ* from *B*-methoxy-9-borabicyclo-[3.3.1]nonane (*B*-OMe-9-BBN) and the corresponding arylmethylzinc bromides. Reduction of **38** and **47** with diisobutylaluminium hydride (DIBALH) afforded **61** and **65**, respectively. Treatment of **38** with phosphorus pentasulfide yielded a thiocarbonyl analog, which was subsequently reacted with $HgCl_2$ and ammonia to give **62**. Compound **63** was prepared using a similar method by heating **38** with phosphorus pentasulfide and ammonia in methanol at 150 °C in a microwave reactor.

Scheme 1[a]

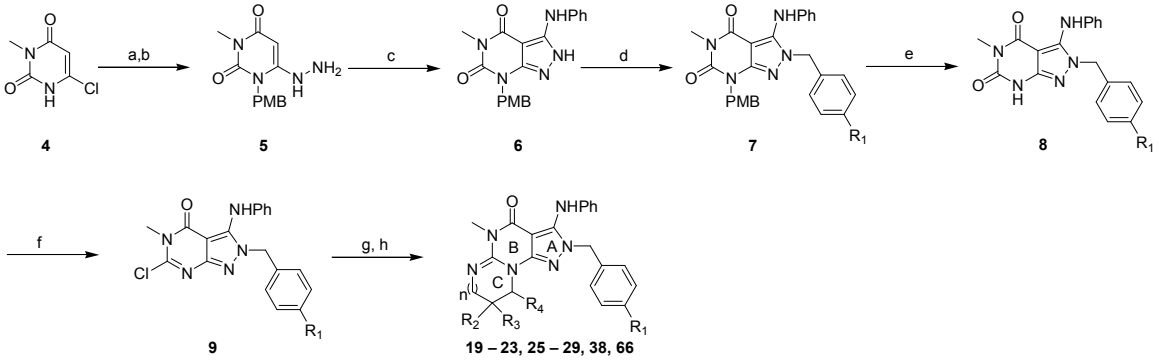

[a] Reagents and conditions: (a) *p*-methoxybenzyl chloride, K_2CO_3, DMF, 60 °C; (b) hydrazine hydrate, EtOH, MeOH, reflux; (c) PhNCS, DMF, 120 °C; (d) $R_1C_6H_4CH_2X$, K_2CO_3, DMF; (e) TFA, TfOH, 25 °C; (f) $POCl_3$, reflux; (g) $HOCHR_4CR_2R_3(CH_2)_nNH_2$, DMF; (h) $SOCl_2$, CH_2Cl_2.

Scheme 2[a]

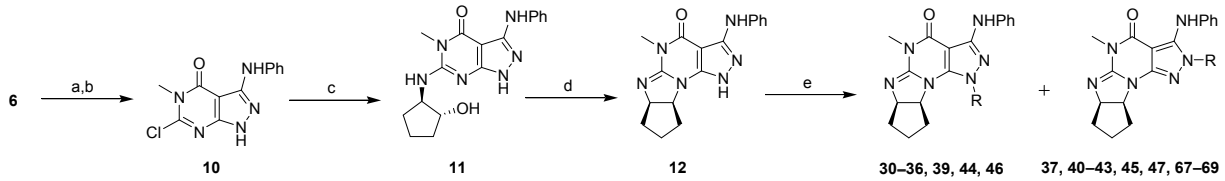

[a] Reagents and conditions: (a) TFA, TfOH, CH_2Cl_2, 25 °C; (b) $POCl_3$, reflux; (c) (1*R*,2*R*)-2-aminocyclopentanol hydrochloride, DIPEA, DMF, 120 °C; (d) $SOCl_2$, CH_2Cl_2; (e) RX, K_2CO_3 or Cs_2CO_3.

Scheme 3[a]

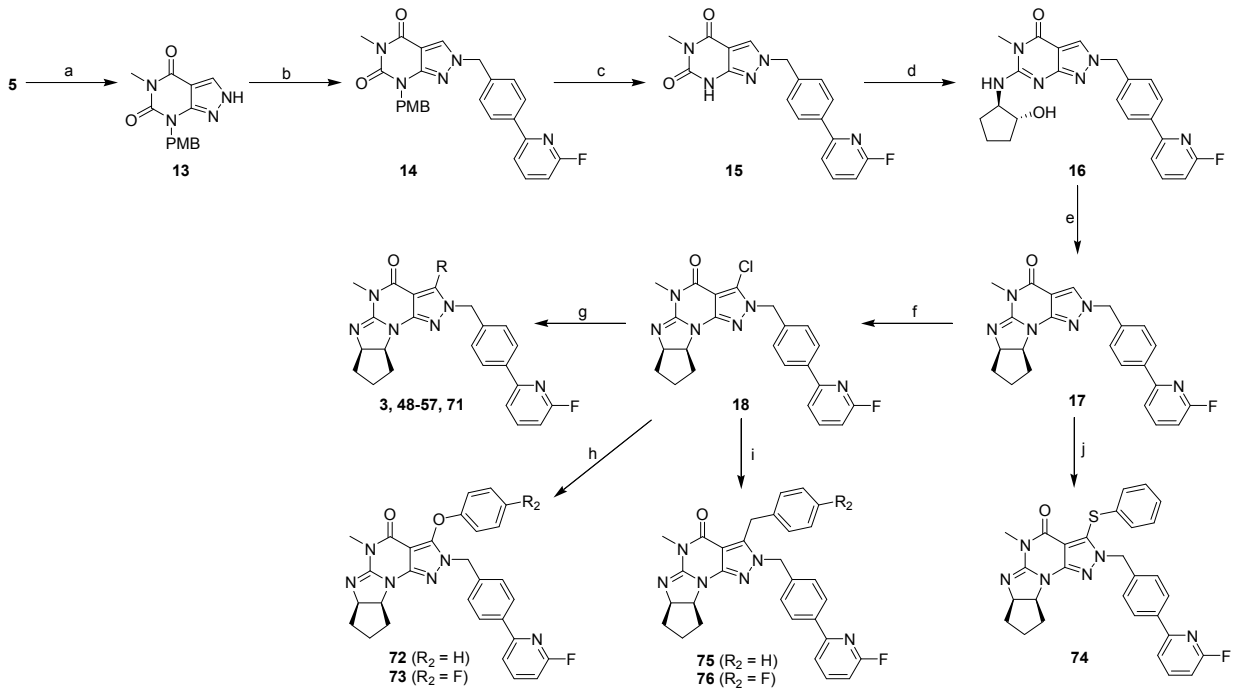

[a] Reagents and conditions: (a) $POCl_3$, DMF; (b) 2-(4-(chloromethyl)phenyl)-6-fluoropyridine, K_2CO_3, DMF, 25 °C; (c) TFA, TfOH, CH_2Cl_2, 25 °C; (d) BOP, DBU, (1*R*,2*R*)-2-aminocyclopentanol hydrochloride, THF, 25 °C; (e) $SOCl_2$, DMF, 25 °C; (f) LiHMDS, C_2Cl_6, THF, 25 °C; (g) alkyl amine, heating; or aryl amine, $Pd_2(dba)_3$, Xantphos, K_2CO_3, *t*-amyl alcohol, reflux; or (hetero)aryl amine,

LiHMDS; (h) ArOH, K_2CO_3, microwave, 150 °C; (i) $ArCH_2ZnX$, B-OMe-9-BBN, PdOAc, S-Phos, DMF, 100 °C; (j) $(PhS)_2$, LiHMDS, THF, 25 °C.

RESULTS AND DISCUSSION

SAR development and X-ray crystallography. As a primary assay for exploring SAR, all of the synthesized compounds were evaluated for their PDE1 inhibitory activities. These compounds were found to be selective for inhibition of PDE1 versus other PDE family members. However, most of the compounds in this series also exhibited weak interactions with PDE4 as an off-target activity. Because of this potential off-target PDE inhibitory activity, a human recombinant PDE4A assay was developed as a counter screen to evaluate compound selectivity for these two enzyme classes. To delineate the SAR around the investigational new drug **3**, four representative sets of compounds were selected as summarized in Tables 1–4.

The SAR of compounds with different ring size and substituents on the C-ring is summarized in Table 1. Compound **19** with a 6-membered C-ring exhibited a PDE1 inhibitory activity of 65 nM. Shrinking the C-ring into a 5-membered ring slightly improved compound inhibitory activity (**21** *vs.* **19**). To establish additional interactions with PDE1, various substituents were introduced on the C-ring. A gem-dimethyl substitution on the C-ring of **19** led to 13-fold increase in PDE1 inhibitory potency and the resulting compound **20** demonstrated over 2000-fold selectivity against PDE4A. Similarly, introduction of a methyl or isopropyl group at the C_a-position of the 5-membered C-ring resulted in 9- and 13-fold increase in PDE1 inhibition activity, respectively (**22** and **23** *vs.* **21**). Hydroxymethyl substituted **24** and tetrahydrofuran-3-yl substituted **25** exhibited 2–5 fold better potency relative to **21** at the expense of approximately 2-fold decrease of selectivity over PDE4A. It appeared that a small hydrophobic alkyl group was preferred at the C_a-position, while a bulky substituent at this position had a detrimental effect on compound binding to PDE1. For instance, C_a-benzyl substituted analog **26** was 13 times less potent in PDE1 inhibition relative to **21**. Conversely, such a structural modification enhanced PDE4A inhibito-

ry potency, with compound **26** showing only 33-fold selectivity over PDE4A. Compound **27**, containing a bulky substituent at the C_a-position, exhibited lesser PDE1 inhibitory potency than **21** as well. We also attempted to introduce a small alkyl group on the C_b-position and found C_b-methylated compound **28** exerted more potent PDE1 inhibitory activity and better selectivity than **21**. To take advantage of the preferred alkyl substitutions at both C_a- and C_b-positions, **29** with a cyclopentyl group fused onto C-ring was synthesized. This compound showed a PDE1 inhibitory activity of 0.85 nM, which was 34-fold more potent than **21**. Among the different sizes of C-ring and substituents, compounds with a cyclopentyl fused 5-membered C-ring demonstrated increased PDE1 inhibitory potency and good selectivity, and therefore compounds with this ring system were selected for further optimizations.

Table 1. SAR of Pyrazolo[3,4-*d*]pyrimidine Derivatives with Variations of Substituents on C-Ring

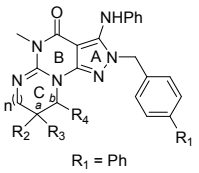

R_1 = Ph

Compd	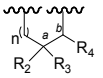	K_i (μM)[a]		Ratio[b]
		PDE1	PDE4A	
19		0.065	> 100	> 1500
20		0.0048	9.9	2063
21		0.029	44	1517
22		0.0033	3.4	1030
23		0.0023	1.5	652
24		0.0060	4.1	683
25	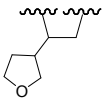	0.014	12	857
26		0.39	13	33
27		0.25	> 100	> 400

28		0.0080	30	3750
29		0.00085	1.3	1529

[a] K_i values are the means of at least two determinations. [b] Ratio of K_i (PDE4A)/K_i (PDE1).

To mimic the ribose moiety of cGMP and create additional interactions with the amino acid residues located in the catalytic site of PDE1, compounds **30**–**47** with various substituents on the pyrazole ring were synthesized, as listed in Table 2. If these compounds and cGMP were to bind to PDE1 in a similar binding pose, substitution at *N*-1 position would correspond to the anchoring position of the ribose group of cGMP. However, compared to the unsubstituted compound **12**, no apparent improvement on PDE1 binding affinity was observed for compounds **30** and **31**, both containing *N*1-substituted alkyl groups. Unexpectedly, the *N*1-(6-fluoropyridin-2-yl)methyl substituted analog **32** exhibited 25-fold increase in PDE4A inhibitory potency while its PDE1 inhibitory potency was only improved 2-fold (**32** *vs.* **12**). Compounds **33**–**35** were designed with an extended linker between the phenyl group and the pyrazolopyrimidinone core, yet this kind of structural modifications had little effect on PDE1 binding affinity. **34** tended to inhibit PDE4A more potently, while the trifluoromethyl analog **35** was a relatively more potent PDE1 inhibitor and demonstrated 33-fold selectivity over PDE4A. An interesting SAR was observed when we compared *N*1- versus *N*2-substituted isomers. Compound **36** was 22 times more potent than **12** in binding to PDE1. Remarkably, its *N*2-substituted isomer **37** exerted over 730-fold increase in PDE1 binding affinity relative to **12** and exhibited over 630-fold selectivity against PDE4A. To follow up on such an interesting finding, a number of compounds with *N*2-substituted analogs were synthesized. Compound **38**, containing a *p*-trifluoromethyl benzyl sidechain at *N*2-position, demonstrated subnanomolar PDE1 binding affinity and excellent selectivity over PDE4A. By replacing the trifluoromethyl group with a hydrophilic methylsulfonyl group, the resulting compound **40** maintained subnanomolar PDE1 inhibitory potency, yet its selectivity over PDE4A decreased 8-fold. Its *N*1-isomer **39** showed similar PDE4A selectivity, but its PDE1 inhibitory activity was weakened 61-fold. Sulfonamide

41 and pyrrolidine derivatives **42** exhibited similar potency and selectivity. *N*-methylation of the pyrrolidine ring had little effect on compound binding profile (**43** *vs.* **42**). By introducing a para-fluoro biphenylmethyl sidechain, the binding affinity of compound **45** was increased over 3400-fold relative to **12**. This sub-nanomolar inhibitor was further optimized by replacing the terminal benzene ring with a 2-pyridyl group to adjust its physicochemical properties. The resulting analog **47** is a picomolar PDE1 inhibitor with a K_i of 85 pM and with over 2800-fold selectivity against PDE4A. The SAR of these compounds clearly demonstrates that *N*2-substitution of the polycyclic compounds is preferred. For instance, **45** and **47** are hundreds of times more potent than their *N*1-isomers, **44** and **46**. In addition, para-substituted benzyl sidechains generally provide compounds with excellent potency and selectivity.

Table 2. SAR of Pyrazolo[3,4-*d*]pyrimidine Derivatives with Variations of Substituents on the A-Ring

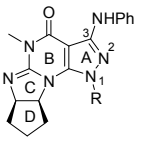

N1-Substitution

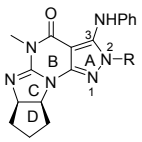

N2-Substitution

Compd	Isomer	R	K_i (μM)[a]		Ratio[b]
			PDE1	PDE4	
12	–	H	1.4	9.8	7.0
30	*N*1		0.77	2.0	2.6
31	*N*1	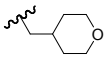	5.0	8.4	1.7
32	*N*1	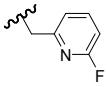	0.67	0.39	0.58
33	*N*1	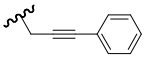	1.1	4.1	3.7
34	*N*1	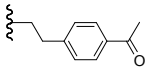	2.0	0.86	0.43
35	*N*1	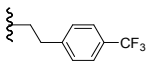	0.54	18	33.3
36	*N*1	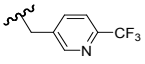	0.065	0.70	11
37	*N*2	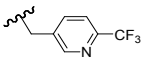	0.0019	1.2	632

38	*N*2	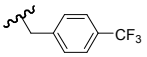	0.00088	0.93	1057
39	*N*1	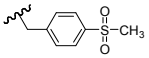	0.030	3.0	100
40	*N*2	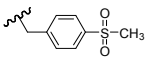	0.00049	0.065	133
41	*N*2	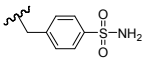	0.0014	1.2	857
42	*N*2	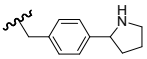	0.0016	1.2	750
43	*N*2	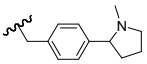	0.0027	3.1	1148
44	*N*1	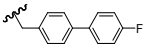	0.24	> 100	> 410
45	*N*2	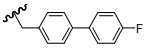	0.00041	0.46	1122
46	*N*1	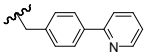	0.042	4.7	112
47	*N*2	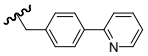	0.000085	0.24	2824

[a] K_i values are the means of at least two determinations. [b] Ratio of K_i (PDE4A)/ K_i (PDE1).

According to the available X-ray structures of PDE enzymes and their binding patterns with cGMP and PDE inhibitors mimicking guanine,[15,16] the *N*-7 nitrogen in the purine ring usually forms a hydrogen bond with an adjacent amino acid residue. Changing the purine ring system into a pyrazolo[3,4-*d*]pyrimidinone scaffold would likely disrupt the hydrogen bond network, especially for the key hydrogen bond with the conserved active-site glutamine, so an amino group was introduced at position 3 of the designed scaffold in an attempt to re-establish a preferred hydrogen bond pattern. To understand the SAR and further improve compound binding profiles, a list of 3-amino substituted compounds were synthesized as shown in Table 3. Compound **48** inhibited PDE1 with a K_i of 5.8 nM. Introducing a methyl group on the NH_2 caused 5-fold decrease of PDE1 binding affinity (**49** *vs.* **48**). Capping the nitrogen with two methyl groups resulted in 21-fold drop in binding potency (**50** *vs.* **48**). Significant lessening of PDE1 binding affinity was also observed for pyrrolidinyl substituted analog **57**, which suggested that the 3-amino group might be involved in the formation of a hydrogen bond and probably served as a hydrogen donor. When a larger alkyl group was substituted on the nitrogen, the PDE1 binding affinity of the resulting compounds, **51**–**54** was improved as the size of the alkyl substituents increased. Similarly,

cyclohexyl substituted **56** showed higher potency than cyclopentyl substituted **55**. Remarkably, compound **3** with a phenylamino group at position 3 exhibited potent PDE1 inhibitory activity (K_i = 58 pM), which was 100-fold more potent than the 3-amino substituted analog **48**. Replacing the phenyl group with a 4-pyridyl group caused over 500-fold decrease in PDE1 binding potency without significant change in the PDE4A binding affinity (**58** *vs.* **3**). Insertion of a methylene group between the NH and benzene ring led to 84-fold decline in PDE1 binding potency (**59** *vs.* **3**). *N*-Methylation of the PhNH group resulted in an over 300-fold drop in PDE1 binding affinity while PDE4A binding potency was largely maintained (**60** *vs.* **47**). It was apparent that an arylamino substituent was preferred at position 3 compared to alkylamino, cycloalkylamino and heteroarylamino groups. An uncapped N-H at this position was essential for binding to PDE1. *N*,*N*-disubstituted analogs gave significantly weaker PDE1 binding affinities.

Table 3. SAR of Pyrazolo[3,4-*d*]pyrimidine Derivatives with Variations of Substituents at Position 3

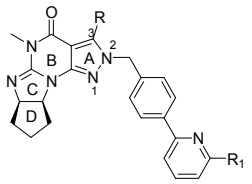

Compd	R	R_1	K_i (μM)[a]		Ratio[b]
			PDE1	PDE4	
48	NH_2	F	0.0058	2.4	414
49	MeNH	F	0.028	4.3	154
50	Me_2N	F	0.12	1.1	9.2
51	^{n}PrNH	F	0.015	6.2	413
52	^{i}PrNH	F	0.012	5.5	458
53	^{i}BuNH	F	0.0074	6.3	851
54	2-methylbutyl-NH	F	0.0013	2.6	2000
55	cyclopentyl-NH	F	0.024	5.5	229
56	cyclohexyl-NH	F	0.0028	1.6	571
57	*N*-pyrrolidinyl	F	0.16	4.6	29
3	PhNH	F	0.000058	0.16	2759

58	4-pyridyl-NH	F	0.031	0.37	12
59	$PhCH_2NH$	F	0.0049	4.0	816
60	PhNMe	H	0.031	0.74	24

[a] K_i values are the means of at least two determinations. [b] Ratio of K_i (PDE4A)/ K_i (PDE1).

We determined the X-ray crystal structure of the catalytic domain of the human recombinant PDE1B complexed with compound **3** to identify interactions between PDE1 and this inhibitor and to further explore SAR around this compound. As shown in Figure 2 and S1A, the pyrazolo[3,4-*d*]pyrimidinone core is held tightly by a "hydrophobic clamp" formed primarily by F424, L388 and F392 located above and below the aromatic core of **3**. The well positioned π–π stacking and hydrophobic interactions between these contact residues and the planar core contribute significantly to the picomolar bind affinity of compound **3**. Compound **3** appears to adopt a binding pose different from that of cGMP.[15,16] In compound **3**, the exocyclic carbonyl group of pyrimidone and the amino group at position 3 form bidentate hydrogen bonds with the *γ*-carboxamide of the conserved Q421 (Figure 3 and S1B). A water-mediated hydrogen bond is observed between the guanidyl nitrogen on the B-ring with the bound metal zinc. The involvement of the N-H group at position 3 of the A-ring in hydrogen bond formation explains our observations that *N,N*-disubstituted compounds, such as **50**, **57** and **60**, were significantly weaker inhibitors than mono-substituted analogs. In addition, replacing this N-H at position 3 with O, S, or CH_2 caused 35–90 fold decrease in PDE1 binding affinity (**72**, **74**–**75** *vs.* **3**), as shown in Table 4. When the key carbonyl group of the B-ring in **38** and **47** was reduced into a methylene group, the PDE1 binding affinities of the resulting analogs **61** and **65** were weakened 50- and 294-fold, respectively. The oxygen of this carbonyl group serves as a hydrogen acceptor in the hydrogen bonding formation with Q421. Converting the carbonyl group into an imine, a hydrogen donor, would prevent the formation of this key hydrogen bond and possibly disrupt other interactions. There was an over 3000-fold decrease in PDE1 binding affinity caused by this structural modification (**62** *vs.* **38**).

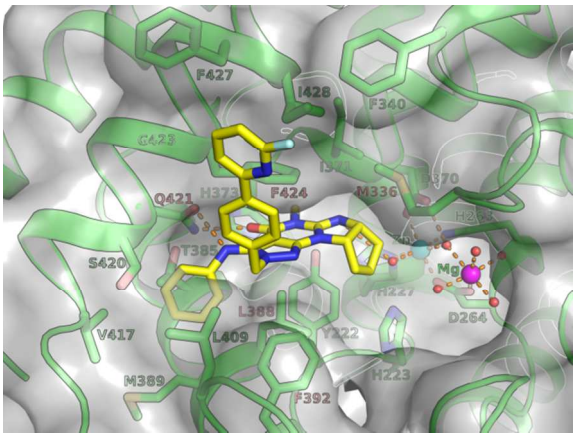

Figure 2. Crystal structure of the catalytic domain of human recombinant PDE1B enzyme complexed with compound 3. Hydrogen bonds between 3 and the invariant Q421 of PDE1B were indicated in orange dashed lines. The pyrazolopyrimidinone core of **3** was sandwiched between residues F424, L388 and F392, forming π–π stacking with F424, π–edge interactions with F392 and hydrophobic interaction with L388.

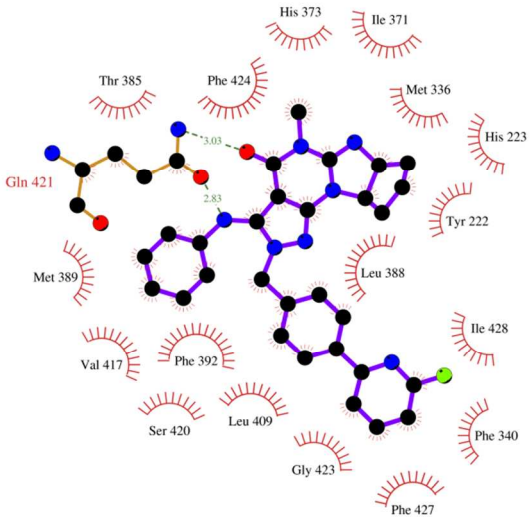

Figure 3. Ligplot presentation of PDE1B complexed with compound 3. Key hydrogen bonds and contact residues located in the catalytic site of PDE1B are highlighted.

The phenylamino group at position 3 of A-ring is buried deeply in a hydrophobic sub-pocket formed primarily by F392, L388, M389, V417, S420, T385 and L409 (Figure S1C). The π–π edge interactions with F392 and additional hydrophobic interactions with these residues provide **3** with greater binding affinity than alkylamino substituted analogs (Table 3 and Figure 2). The cyclopentyl group fused on the C-ring with a stereochemistry of (6a*R*, 9a*S*) bends down and fits nicely into the catalytic pocket and has van der Waals interactions with M336 and several other residues. Compounds **3** and its close analog **47** exhibited 62- and 93-fold higher affinity than the corresponding enantiomers **70** and **66** with the ring fusion carbons adopting (6a*S*, 9a*R*) configuration. These enantiomers may not fit in the binding pocket well since the cyclopentyl moiety of these molecules may collide with the amino acid residues in the adjoining catalytic pocket primarily formed by M336, H223 and I371, and consequently forcing the compounds to adopt less favorable binding poses. The *N*-methyl group at position 5 inserts into a small cavity, surrounded by I371, H373, F424 and Y222 (Figure 3). The additional interactions of the *N*-methyl group with these residues supports the observed SAR that *N*-methylated compound **38** was 330 times more potent in PDE1 inhibitory activity than its desmethyl analog **63**. Interestingly, *N*-demethylation did not cause significant change in the PDE4 inhibitory potency. Compound **63** became a PDE1 and PDE4A dual inhibitor by way of losing PDE1 inhibitory activity, as shown in Table 4. The *N*-methyl group will prevent potential tautomerization of the pyrimidone B-ring into pyrimidinol,[24] which would disrupt the important hydrogen bonding of the exocyclic carbonyl group with Q421. The phenylene and pyridyl groups of the 4-(6-fluoropyridin-2-yl)benzyl sidechain of **3** each had π–π interactions with F424 and F427, respectively, in addition to various van der Waals interactions with other residues such as G423, S420, F340 and I428 (Figure 2, 3 and S1D). These additional interactions created by the *N*2-substituted sidechain provide **3** with over 24000 times more potent binding affinity to PDE1 relative to unsubstituted analog **12**. It was evident that the observed SAR of these polycyclic pyrazolopyrimidinones and the key interactions between PDE1B and the bound ligand **3** revealed by the crystal structure described above are well correlated with each other. The planar pyrazolopyrimidinone core, 3-phenylamino group, *para*-substituted benzyl sidechain at *N*2-position and the fused cyclopentyl

group with an absolute configuration of (6a*R*, 9a*S*), all provide major contributions to the sub-nanomolar PDE1 binding potency of this series of compounds.

Table 4. SAR of Tetracyclic Pyrazolo[3,4-*d*]pyrimidine Derivatives.

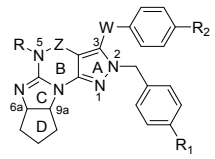

Compd	Z	W	R	Stereochemistry		R_1	R_2	K_i (μM) [a]		Ratio [b]	HLM Cl_{int} (ml/min/kg)
				6*a*	9*a*			PDE1	PDE4A		
61	CH_2	NH	Me	R	S	CF_3	H	0.044	37	841	64
62	C=NH	NH	Me	R	S	CF_3	H	2.8	18	6.4	32
38	C=O	NH	Me	R	S	CF_3	H	0.00088	0.93	1057	139
63	C=O	NH	H	R	S	CF_3	H	0.29	0.55	2	22
64	C=O	NH	Me	R	S	CF_3	F	0.00063	0.42	667	73
47	C=O	NH	Me	R	S	pyridin-2-yl	H	0.000085	0.24	2824	189
65	CH_2	NH	Me	R	S	pyridin-2-yl	H	0.025	18	720	59
66	C=O	NH	Me	S	R	pyridin-2-yl	H	0.0053	8.4	1585	72
67	C=O	NH	Me	R	S	3-fluoropyridin-2-yl	H	0.000073	0.20	2740	276
68	C=O	NH	Me	R	S	4-fluoropyridin-2-yl	H	0.000062	0.33	5323	218
69	C=O	NH	Me	R	S	5-fluoropyridin-2-yl	H	0.000074	0.50	6757	125
3	C=O	NH	Me	R	S	6-fluoropyridin-2-yl	H	0.000058	0.16	2759	78
70	C=O	NH	Me	S	R	6-fluoropyridin-2-yl	H	0.0054	8.4	1556	51
71	C=O	NH	Me	R	S	6-fluoropyridin-2-yl	F	0.00015	0.062	413	107
72	C=O	O	Me	R	S	6-fluoropyridin-2-yl	H	0.0030	0.25	83	214
73	C=O	O	Me	R	S	6-fluoropyridin-2-yl	F	0.0066	0.22	33	266
74	C=O	S	Me	R	S	6-fluoropyridin-2-yl	H	0.0052	0.93	179	208
75	C=O	CH_2	Me	R	S	6-fluoropyridin-2-yl	H	0.0022	0.77	350	165
76	C=O	CH_2	Me	R	S	6-fluoropyridin-2-yl	F	0.0023	0.78	339	81

[a] K_i values are the means of at least two determinations. [b] Ratio of K_i (PDE4A)/ K_i (PDE1).

Table 5. PDE Family Selectivity of Selected PDE1 Inhibitors.

Compd	K_i (μM) [a]										
	PDE1	PDE2A	PDE3B	PDE4A	PDE5A	PDE6	PDE7B	PDE8A	PDE9A	PDE10A	PDE11A
29	0.00085	37	1.5	1.3	1.6	1.1	0.91	33	>100	7.9	7.1
47	0.000085	24	1.2	0.24	0.60	0.43	0.30	8.2	6.1	2.7	2.6
38	0.00088	39	30	0.93	0.59	1.6	1.2	54	50	5.4	28
37	0.0019	> 100	42	1.2	1.2	5.5	6.1	> 100	> 100	19	72
3	0.000058	18	3.1	0.16	0.63	0.32	0.36	3.0	17	1.8	1.3

[a] K_i values are the means of at least two determinations.

Metabolic stability, profiling and pharmacokinetics. Metabolic stability studies using human liver microsomes (HLM) showed that the sub-nanomolar PDE1 inhibitors **38** and **47** process relatively high

microsomal clearance, as shown in Table 4. Their analogs, **62**, **63** and **65**, exhibited lower HLM clearance, but with a significant loss in PDE1 binding potency. To improve compound metabolic stability while maintaining potency, the *para*-position of the potentially metabolically labile phenylamino group at position 3 of the A-ring was capped with a fluoro group. The fluoro-capped analog **64** showed similar potency with **38**, and demonstrated slightly lower HLM clearance. A similar trend was observed for the 3-benzyl substituted pair of compounds **75** and **76**. Clearance of para-fluoro analog **73**, however, was not improved over **72**. Fluorination of the phenylamino group on the A-ring of compound **3** caused a 7-fold drop in PDE4A selectivity and a slight decrease in PDE1 binding potency, without a significant effect on microsomal stability (**71** *vs.* **3**). Another attempt to improve metabolic stability was made by a fluorine scan of the 4-(pyridin-2-yl)benzyl group, which was the preferred sidechain at the *N*2 position, enabling **47** to bind to PDE1 with an K_i of 0.000085 μM. Compounds **67**–**69** and **3** with a fluoro group substituted at different positions of the pyridine ring were evaluated in the HLM stability assay. Compound **3** demonstrated relatively lower clearance than **47** and other fluorinated analogs while maintaining great potency and selectivity, as shown in Tables 4 and 5. Compounds **3** and **47** both exhibited excellent selectivity over other PDE family members. These compounds did not show meaningful PDE1 sub-type selectivity. For instance, the K_i values of compound **3** against recombinant full-length human PDE1A, PDE1B and PDE1C are 0.000033 μM, 0.00038 μM and 0.000035 μM, respectively. Compound **3** was profiled in a panel of enzymes, receptors, transporters and ion channels from Caliper at 10 μM, which was over 170,000 times higher than its K_i for PDE1, and demonstrated good selectivity.

Table 6. Physicochemical and Pharmacokinetic Properties of Selected PDE1 Inhibitors.

Compd		**29**	**47**	**41**	**38**	**64**	**74**	**72**	**73**	**75**	**76**	**3**
LogD at pH 7.4		>5	3.54	1.96	4.47	4.57	> 5	4.61	4.77	4.96	>5	4.41
LogD at pH 1.7		1.92	-0.58	-0.96	1.16	1.11	2.49	1.05	1.21	1.36	1.42	1.27
Solubility in PBS (μM)		2	>100	>100	35	31	<1	8	7	<1	<1	22
Mouse PK parameters [a]												
Plasma Cmax(obs) (ng/mL)		130	48	650	60	21	93	165	88	86	44	490
Brain Cmax(obs) (ng/mL)		474	28	16	285	133	71	170	64	101	81	387
Plasma AUC_{last} (ng-h/mL)		286	65	785	122	24	108	210	119	134	69	826
Brain AUC_{last} (ng-h/mL)		542	21	15	548	166	81	192	102	154	109	588
Brain/Plasma ratio [b]		2.9	0.3	0.02	4.5	6.9	0.8	0.9	0.9	1.2	1.6	0.7
Rat PK parameters [c]												
iv	$t_{1/2}$ (h)		0.72		1.4	1.5						1.4
	Vd (L/kg)		2.48		7.44	7.48						6.83
	CL (mL/min/kg)		40		62	57						55
	AUC_{∞} (ng-h/mL)		420		271	292						300
po	$t_{1/2}$ (h)	3.1	1.5		1.5	2.2						1.5
	C_{max} (ng/mL)	102	158		75	42						252
	Tmax (obs) (h)	4.0	0.50		0.25	0.50						0.75
	AUC_{∞} (ng-h/mL)	816	636		214	164						802
	F (%)		16		8	6						28

[a] Screening mode PK studies in male C57BL/6 mice. Compounds in 0.05M pH 4.0 citrate buffer containing 5% Labrasol and 5% TPGS were administered to mice at 10 mg/kg via oral gavage. [b] Ratio of brain $AUC_{0\text{-}2h}$/plasma $AUC_{0\text{-}2h}$. [c] Male Sprague-Dawley rats were administered with test compounds in 0.05M pH 3.1 citrate-phosphate buffer at 1 mg/kg by intravenous injection or in 0.02 N HCl at 9.75 mg/kg by oral gavage.

The pharmacokinetic properties of selected compounds were evaluated in mice after oral administration, as summarized in Table 6. All of the tested compounds were orally bioavailable. The sub-nanomolar PDE1 inhibitor **29** exhibited good brain exposure with a brain to plasma ratio of 2.9, but this hydrophobic compound has poor physicochemical properties, as shown in Table 6, and was not suitable for further development. When a nitrogen was introduced into the terminal phenyl ring on the sidechain of **29**, the resulting compound **47** showed 10 times more potent PDE1 binding affinity. Moreover, **47** exhibited much better solubility in PBS buffer and had appropriate physicochemical properties for a CNS drug candidate, as shown in Table 6. The plasma and brain exposure of this compound is lower than that of **29** giving it a brain to plasma ratio of 0.3. Compound **47** has two basic pKa′s (7.0 and 4.3). In contrast, compound **3** has a single basic pKa (7.0), as fluorination on the α-carbon of the pyridine ring prevents ionization of the sidechain. The fine-tuning of physicochemical and ionization properties provided **3** with improved brain exposure and better metabolic stability in human liver microsomes, as well

as a preferred brain to plasma ratio of 0.7 in mice after oral dosing. Oral bioavailability of compounds in Table 6 was determined in a screening mode using one formulation. In general, formulations can be optimized further on a compound-specific basis. Compound **3** exhibited higher bioavailability than **47** in rats, as shown in Table 6. Compound **41** is a more hydrophilic compound with a LogD of 1.96 at pH7.4 and a large topological polar surface area (TPSA, 134 $Å^2$) due to the polar sulfonamide group on the sidechain. These properties result in this compound having very good plasma exposure, but limited brain penetration (brain/plasma ratio = 0.02). Such a compound is suitable for non-CNS indications. The hydrophobic analog **38** with a *p*-trifluorobenzyl sidechain exhibited a brain to plasma ratio of 4.5 in mice, but this compound has high clearance rates both *in vivo* and in human liver microsomes. Compound **38** showed low oral bioavailability in rats (Table 6). Capping the *para*-position of the potentially metabolically labile phenylamino group with a fluoro group resulted in relatively lower oral exposure (**64** *vs.* **38**). Replacing the key phenylamino group of **3** with an arylthio, aryloxy or benzyl group not only led to decreased PDE1 inhibitory potency, but also resulted in poor physicochemical properties and low plasma and brain exposure after oral administration in mice (**72**–**76** *vs.* **3**). Among all of these tested compounds, compound **3** possesses a good overall profile with balanced physicochemical properties, excellent potency and selectivity and good pharmacokinetics.

***In vivo* Studies.** Compound **3** was studied in various animal models of motor and cognitive functions to evaluate its *in vivo* efficacy before being nominated for clinical development. As one of the proof of concept studies, compound **3** was evaluated for effects on memory performance using the rat novel object recognition (NOR) test. Compound **3** was found to significantly enhance memory performance in the test with a minimum effective dose of 3 mg/kg (Figure 4). As is customary in this assay, an inverted U-shaped dose response curve was observed.[25] An extensive pharmacological profiling of compound **3** using animal models of cognitive dysfunction and other CNS disorders has been conducted and com-

pound **3** exhibited good efficacy in these models after oral administration. These results will be reported elsewhere.

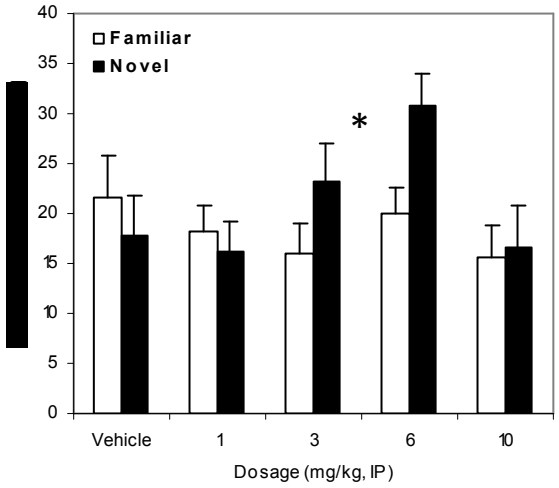

Figure 4. Effect of compound 3 on cognitive performance of male Sprague-Dawley rats in the novel object recognition task. Data are expressed as mean (with SEM). * indicates a statistical difference between the familiar and novel object ($p < 0.05$).

CONCLUSION

A novel series of 3-aminopyrazolo[3,4-*d*]pyrimidinones has been designed and synthesized as PDE1 inhibitors. Systematic optimization of this scaffold led to the discovery of compound **3**, a picomolar PDE1 inhibitor with excellent selectivity against the members of other PDE families, PDE2 – 11. The interactions between compound **3** and the contact residues located in the catalytic pocket of PDE1 were elucidated based upon the observed SAR and the high resolution crystal structure of PDE1B complexed with compound **3**. Compound **3** possesses good physicochemical and pharmacokinetic properties for a CNS-active drug candidate, and showed efficacy in various animal models of motor and cognitive functions. In multiple human Phase 1 clinical trials compound **3** has demonstrated a favorable safety profile and has been generally well-tolerated across a broad range of doses both in healthy volunteers and in

patients with schizophrenia. The pharmacokinetic profile of compound **3** supports once daily dosing, being rapidly absorbed with a mean plasma half-life of approximately 14 to 18 hours. More detailed preclinical and clinical results of **3** will be reported in other forums.

EXPERIMENTAL SECTION

Chemistry. Unless otherwise noted, all materials were obtained from commercial suppliers and used without further purification. All reactions involving air- or moisture-sensitive reagents were performed under an argon atmosphere. All microwave assisted reactions were conducted with an Initiator™ Eight EXP Microwave System from Biotage, Charlotte, NC, USA. Silica gel or alumina column chromatography was performed with a CombiFlash Companion purification system from Teledyne ISCO, Lincoln, NE. All compounds synthesized, unless otherwise noted, were purified by column chromatography and/or preparative reverse–phase HPLC. A Waters preparative HPLC system equipped with a Delta 600EF pump, 2996 PDA detector and WFCIII fraction collector was used for compound purification using the following general HPLC method. Column: Gemini, AXIA packed, 10 μm C18 110Å, 250 × 21.2 mm; mobile phase A, 0.1% formic acid in water; mobile phase B, 0.1% formic acid in acetonitrile; gradient was adjusted and optimized based on compound polarity; run time 22 min; flow rate 24 mL/min; detection at 210–350 nm. ^{1}H-NMR spectra were determined in the cited solvent on a Bruker DRX 300 or Avance III (400 MHz or 500 MHz) spectrometer. ^{13}C NMR spectra were recorded at 75 or 126 MHz. Chemical shifts are reported in delta (δ) units, parts per million (ppm) downfield from tetramethylsilane. Coupling constants are reported in hertz (Hz). Splitting patterns are designated as follows: s, singlet; br, broad singlet; d, doublet; t, triplet; q, quartet; m, multiplet. Purity of all final products was > 95% as determined by reverse–phase HPLC on a Waters Alliance 2695 system with a 2996 PDA detector. HPLC method: Column, XBridge Shield RP18 column, 150 mm × 4.6 mm, 5 μm, 30 °C; mobile phase A, 0.02 mol/L phosphate buffer (pH 6.8)/acetonitrile (13/7, v/v); mobile phase B, acetonitrile/0.02 mol/L phosphate buffer (pH 6.8) (7/3, v/v); gradient, 0.0–30 min, 0–100% B; 30–30.1 min, 100–0% B;

30.1–40 min, 0% B; flow rate 1.0 mL/min; detection at 225 nm. Mass spectral (MS) data were determined on a Micromass Quattro micro API Mass, or LCT Premier XE spectrometer from Waters. The chemical yields reported below are not optimized and correspond as specific examples of a single preparation.

Representative synthetic procedures of polycyclic pyrazolopyrimidine derivatives shown in Scheme 1. 2-(Bi-phenyl-4-ylmethyl)-7,8,9-trihydro-5-methyl-3-(phenylamino)-[2*H*]-pyrazolo[4,3-*e*]pyrimido-[1,2-*a*]pyrimidin-4(5*H*)-one (19). *Step a. 6-Chloro-1-(4-methoxybenzyl)-3-methylpyrimidine-2,4(1H,3H)-dione.* A mixture of 6-chloro-3-methylpyrimidine-2,4(1*H*,3*H*)-dione (**4**) (8.46 g, 52.7 mmol), *p*-methoxybenzyl chloride (7.9 mL, 58.2 mmol) and potassium carbonate (7.3 g, 58.9 mmol) in anhydrous DMF (100 mL) was heated at 60 °C for an hour. After hot filtration, the filtrate was evaporated to dryness under reduced pressure. The residue was crystallized from hexane to give crude 6-chloro-1-(4-methoxybenzyl)-3-methylpyrimidine-2,4(1*H*,3*H*)-dione as a yellowish crystalline solid (13.8 g, 93% yield), which was used directly in the next step without further purification. A small amount of the crude material was further purified by silica-gel column chromatography using a gradient of 0 – 50% ethyl acetate in hexane as eluent to afford the pure product as a crystalline solid. ^{1}H NMR (500 MHz, $CDCl_3$) δ 7.30 (d, J = 8.6 Hz, 2H), 6.87 (d, J = 8.6 Hz, 2H), 5.93 (s, 1H), 5.21 (s, 2H), 3.80 (s, 3H), 3.35 (s, 3H). MS (ESI) *m/z* 281.1 $[M+H]^+$.

*Step b. 6-Hydrazinyl-1-(4-methoxybenzyl)-3-methylpyrimidine-2,4(1H,3H)-dione (**5**).* To a solution of the crude 6-chloro-1-(4-methoxybenzyl)-3-methylpyrimidine-2,4(1*H*,3*H*)-dione (2.4 g, 8.6 mmol) in EtOH (25 mL) and MeOH (50 mL) was added anhydrous hydrazine (1.2 mL). The reaction mixture was refluxed for 3 h and then cooled to room temperature. A large amount of ether was added into the reaction mixture and then filtered. The filter cake was dried under vacuum to give the title compound as a crystalline solid (2.0 g, 84% yield). ^{1}H NMR (500 MHz, DMSO-d_6) δ 8.07 (s, 1H), 7.15 (d, J = 8.5 Hz, 2H), 6.88 (d, J = 8.5 Hz, 2H), 5.14 (s, 1H), 5.02 (s, 2H), 4.40 (br, 2H), 3.72 (s, 3H), 3.12 (s, 3H). MS (ESI) *m/z* 277.1 $[M+H]^+$.

*Step c. 7-(4-Methoxybenzyl)-5-methyl-3-phenylamino-2H-pyrazolo[3,4-d]pyrimidine-4,6(5H,7H)-dione (**6**).* To a suspension of 6-hydrazinyl-1-(4-methoxybenzyl)-3-methylpyrimidine-2,4(1*H*,3*H*)-dione (10.1 g, 36.6 mmol) in DMF (100 mL) was added phenyl isothiocyanate (19.8 g, 14.7 mmol). The reaction mixture was heated at 115°C for 3 days and then evaporated to dryness under reduced pressure. The residue was washed with hexane (2 × 200 mL) and then crystallized from methanol to give the title compound as a crystalline solid (9.9 g, yield, 72%). ^{1}H NMR (500 MHz, $CDCl_3$) δ 7.53 (s, 1H), 7.43 (d, J = 8.7 Hz, 2H), 7.40 – 7.34 (m, 2H), 7.20 (d, J = 8.4 Hz, 2H), 7.18 – 7.12 (m, 1H), 6.83 (d, J = 8.8 Hz, 2H), 5.05 (s, 2H), 3.77 (s, 3H), 3.35 (s, 3H). MS (ESI) *m/z* 378.3 $[M+H]^+$.

*Step d. 2-(Biphenyl-4-ylmethyl)-7-(4-methoxybenzyl)-5-methyl-3-(phenyl-amino)-2H-pyrazolo[3,4-d]pyrimidine-4,6(5H,7H)-dione (**7**; R_1 = Ph).* To a solution of 7-(4-methoxybenzyl)-5-methyl-3-phenylamino-2*H*-pyrazolo[3,4-*d*]pyrimidine-4,6(5*H*,7*H*)-dione (24 mg, 0.064 mmol) and 4-(bromomethyl)biphenyl (17 mg, 0.070 mmol) in acetone (3.0 mL) was added potassium carbonate (8.8 mg, 0.064 mmol). The reaction mixture was stirred at room temperature overnight. After the solvent was removed under reduced pressure, the residue was purified by silica-gel column chromatography using a gradient of 0 – 75% ethyl acetate in hexane as eluent to afford the title compound as a white solid (24 mg, 69% yield). ^{1}H NMR (300 MHz, $CDCl_3$) δ 7.56 (d, J = 7.4 Hz, 2H), 7.52 – 7.39 (m, 6H), 7.39 – 7.26 (m, 3H), 7.15 – 7.02 (m, 3H), 6.94 (d, J = 7.8 Hz, 2H), 6.85 – 6.70 (m, 3H), 5.10 (s, 2H), 4.99 (s, 2H), 3.72 (s, 3H), 3.32 (s, 3H). MS (ESI) *m/z* 544.3 $[M+H]^+$.

*Step e. 2-(Biphenyl-4-ylmethyl)-5-methyl-3-phenylamino-2H-pyrazolo[3,4-d]pyrimidine-4,6(5H,7H)-dione (**8**; R_1 = Ph).* To a solution of 2-(biphenyl-4-ylmethyl)-7-(4-methoxybenzyl)-5-methyl-3-(phenyl-amino)-2*H*-pyrazolo[3,4-*d*]pyrimidine-4,6(5*H*,7*H*)-dione (3.4 g, 6.25 mmol) in trifluoroacetic acid (28 mL) was added trifluoromethanesulfonic acid (1.11 mL, 12.5 mmol). The reaction mixture was stirred at room temperature overnight. After TFA was removed under reduced pressure, the residue was treated with water (100 mL), followed by 28% ammonium hydroxide (10 mL). The resulting precipitate was filtered, washed with water (4 × 50 mL), and then dried under vacuum. The obtained crude product was

further purified by silica-gel column chromatography using a gradient of 0 – 100% ethyl acetate in hexane as eluent to afford the title compound as a white solid (2.6 g, 96% yield). ^{1}H NMR (500 MHz, $CDCl_3$) δ 9.22 (s, 1H), 7.52 (d, J = 7.7 Hz, 2H), 7.46 (d, J = 8.1 Hz, 2H), 7.44 – 7.38 (m, 2H), 7.38 – 7.28 (m, 3H), 7.16 – 7.11 (m, 1H), 7.08 (d, J = 8.1 Hz, 2H), 6.97 (d, J = 8.0 Hz, 2H), 6.83 (s, 1H), 5.01 (s, 2H), 3.33 (s, 3H). MS (ESI) *m/z* 424.2 $[M+H]^+$.

*Step f. 2-(Biphenyl-4-ylmethyl)-6-chloro-5-methyl-3-(phenylamino)-2H-pyrazolo[3,4-d]pyrimidin-4(5H)-one (**9**; R_1 = Ph).* 2-(Biphenyl-4-ylmethyl)-5-methyl-3-phenylamino-2*H*-pyrazolo[3,4-*d*]pyrimidine-4,6(5*H*,7*H*)-dione (2.4 g, 5.67 mmol) was suspended in $POCl_3$ (80 mL). The mixture was heated at reflux overnight and then evaporated under reduced pressure. The residue was treated with water and ethyl acetate and then adjusted to pH = 9 with 28% ammonium hydroxide. The aqueous phase was extracted with ethyl acetate (3 × 100 mL), and the combined organic phase was evaporated to dryness. The residue was purified by silica-gel column chromatography using a gradient of 0 – 75% ethyl acetate in hexane as eluent to afford the title compound as a white solid (1.4 g, 56% yield). ^{1}H NMR (500 MHz, $CDCl_3$) δ 7.53 (d, J = 7.6 Hz, 2H), 7.50 – 7.39 (m, 4H), 7.37 – 7.32 (m, 1H), 7.31 – 7.26 (m, 2H), 7.14 (d, J = 8.1 Hz, 2H), 7.11 – 7.04 (m, 1H), 6.84 (d, J = 7.9 Hz, 2H), 6.43 (s, 1H), 5.17 (s, 2H), 3.61 (s, 3H). MS (ESI) *m/z* 442.2 $[M+H]^+$.

Step g. 2-(Biphenyl-4-ylmethyl)-6-(3-hydroxypropylamino)-5-methyl-3-phenylamino-2H-pyrazolo[3,4-d]pyrimidin-4(5H)-one. A mixture of 2-(biphenyl-4-ylmethyl)-6-chloro-5-methyl-3-phenylamino-2*H*-pyrazolo[3,4-*d*]pyrimidin-4(5*H*)-one (100 mg, 0.23 mmol), 3-aminopropan-1-ol (85 μL, 1.1 mmol) and *N,N-di*isopropylethylamine (200 μL, 1.1 mmol) in DMF (3.0 mL) was heated at 110 °C overnight. After the solvent was removed under reduced pressure, the residue was purified with a Waters semi-preparative HPLC system using a gradient of 0 – 60% acetonitrile in water containing 0.1% formic acid over 16 min to afford the title compound as a white solid (80 mg, 73% yield). ^{1}H NMR (500 MHz, $CDCl_3$) δ 7.52 (d, J = 7.2 Hz, 2H), 7.47 – 7.38 (m, 4H), 7.36 – 7.29 (m, 1H), 7.28 – 7.24 (m, 2H), 7.15 (d, J = 8.1 Hz, 2H), 7.06 – 6.98 (m, 1H), 6.84 (d, J = 7.8 Hz, 2H), 6.48 (s, 1H), 5.85 (br, 1H), 5.09 (s,

2H), 3.79 (t, J = 5.4 Hz, 2H), 3.75 – 3.68 (m, 2H), 3.36 (s, 3H), 1.94 – 1.81 (m, 2H). MS (ESI) *m/z* 481.2 $[M+H]^+$.

*Step h. 2-(Biphenyl-4-ylmethyl)-7,8,9-trihydro-5-methyl-3-(phenylamino)-[2H]-pyrazolo[4,3-e]pyrimido-[1,2-a]pyrimidin-4(5H)-one (**19**; R_1 = Ph, R_2 = R_3 = R_4 = H, n = 1).* To a solution of thionyl chloride (9.0 μL, 0.10 mmol) in methylene chloride (3.0 mL) was added 2-(biphenyl-4-ylmethyl)-6-(3-hydroxy propyl amino)-5-methyl-3-phenylamino-2*H*-pyrazolo[3,4-*d*]pyrimidin-4(5*H*)-one (25 mg, 0.052 mmol) at 0 °C. The reaction mixture was warmed to room temperature and stirred overnight. After the solvent was removed under reduced pressure, the residue was purified with a Waters semi-preparative HPLC system using a gradient of 0 – 35% acetonitrile in water containing 0.1% formic acid over 16 min to afford the final compound as an off-white solid (13 mg, 54% yield). ^{1}H NMR (500 MHz, $CDCl_3$) δ 7.52 (d, J = 7.4 Hz, 2H), 7.46 (d, J = 8.2 Hz, 2H), 7.44 – 7.38 (m, 2H), 7.37 – 7.31 (m, 1H), 7.30 – 7.23 (m, 2H), 7.11 (d, J = 8.2 Hz, 2H), 7.08 – 7.02 (m, 1H), 6.91 (d, J = 7.8 Hz, 2H), 5.11 (s, 2H), 3.96 (t, J = 6.0 Hz, 2H), 3.69 (t, J = 5.7 Hz, 2H), 3.26 (s, 3H), 2.07 – 1.93 (m, 2H). MS (ESI) *m/z* 463.2 $[M+H]^+$. HRMS (ESI) *m/z* calcd for $C_{28}H_{27}N_6O$ $[M+H]^+$: 463.2246; found: 463.2260. HPLC purity: 98.7%; retention time: 13.7 min.

Representative synthetic procedures of pyrazolo-pyrimidinones shown in Scheme 2. (6a*R*,9a*S*)-5,6a,7,8,9,9a-hexahydro-1-(cyclopentylmethyl)-5-methyl-3-phenylamino-cyclopent[4,5]imidazo[1,2-*a*]pyrazolo[4,3-*e*]pyrimidin-4(1*H*)-one (30). *Step a and b. 6-Chloro-5-methyl-3-phenylamino-1H-pyrazolo[3,4-d]pyrimidin-4(5H)-one (**10**)* To a solution of 7-(4-methoxybenzyl)-5-methyl-3-phenylamino-1*H*-pyrazolo[3,4-*d*]pyrimidine-4,6(5*H*,7*H*)-dione (6.6 g, 17.5 mmol) in CH_2Cl_2 (200 mL) was added TFA (30 mL) slowly at room temperature, followed by trifluoromethanesulfonic acid (10 mL). After the addition was completed, the reaction mixture was stirred at room temperature for 2 h. The solvent was removed under reduced pressure, and then 200 mL of 1.0 N NaOH was added at 0 °C. The mixture was extracted with ethyl acetate five times (5 × 100 mL). The combined organic phase was dried over Na_2SO_4, and then filtered. The filtrate was evaporated to dry-

ness to give 5-methyl-3-(phenylamino)-2*H*-pyrazolo[3,4-*d*]pyrimidine-4,6(5*H*,7*H*)-dione as a white solid (4.3 g, yield 96%). MS (ESI) *m/z* 258.1 $[M+H]^+$. The crude 5-methyl-3-(phenylamino)-2*H*-pyrazolo[3,4-*d*]pyrimidine-4,6(5*H*,7*H*)-dione (4.3 g, 16.7 mmol) was suspended in $POCl_3$ (120 mL), and then heated at reflux for 2 days. After $POCl_3$ was removed under reduced pressure, the residue was suspended in 100 mL of water and carefully adjusted to pH = 1 – 2 with 7.0 % NH_4OH at 0 °C. The mixture was then extracted with CH_2Cl_2/MeOH (10:1, v/v) five times (5 × 100 mL). The combined organic phase was washed with water (2 × 50 mL), dried over Na_2SO_4, and then evaporated under reduced vacuum to give crude 6-chloro-5-methyl-3-phenylamino-1*H*-pyrazolo [3,4-*d*]pyrimidin-4(5*H*)-one (3.3 g, yield: 72%). A small amount of the crude material was further purified by semi-preparative reverse–phase HPLC using a gradient of 0 – 55% of acetonitrile in water with 0.1% formic acid as eluent to afford the pure product as a white solid. ^{1}H NMR (500 MHz, DMSO-d_6) δ 12.98 (s, 1H), 7.96 (s, 1H), 7.67 (d, J = 8.1 Hz, 2H), 7.33 – 7.18 (m, 2H), 6.91 – 6.81 (m, 1H), 3.57 (s, 3H). MS (ESI) *m/z* 276.1 $[M+H]^+$.

*Step c. 6-((1R,2R)-2-Hydroxycyclopentylamino)-5-methyl-3-phenylamino-1H-pyrazolo[3,4-d]pyrimidin-4(5H)-one (**11**).* A solution of 6-chloro-5-methyl-3-phenylamino-1*H*-pyrazolo[3,4-*d*] pyrimidin-4(5*H*)-one (140 mg, 0.51 mmol), (1*R*,2*R*)-2-amino cyclopentanol hydrochloride (280 mg, 2.0 mmol) and *N,N*-diisopropylethylamine (0.44 mL, 2.5 mmol) in DMF (3.0 mL) was heated at 120 °C overnight. After the solvent was removed under reduced pressure, the residue was purified by silica-gel column chromatography using a gradient of 0 – 25% methylene chloride/methanol (5/1, v/v) in hexane as eluent to afford the title compound as an off-white solid (157 mg, 91% yield). ^{1}H NMR (500 MHz, DMSO-d_6) δ 11.97 (s, 1H), 7.73 – 7.57 (m, 3H), 7.30 – 7.18 (m, 2H), 6.86 – 6.79 (m, 1H), 6.76 (d, J = 6.4 Hz, 1H), 4.81 (d, J = 3.8 Hz, 1H), 4.18 – 3.93 (m, 2H), 3.34 (s, 3H), 2.16 – 2.01 (m, 1H), 1.99 – 1.81 (m, 1H), 1.74 – 1.60 (m, 2H), 1.58 – 1.38 (m, 2H). MS (ESI) *m/z* 341.2 $[M+H]^+$.

*Step d. (6aR,9aS)-5,6a,7,8,9,9a-Hexahydro-5-methyl-3-(phenylamino)-cyclopent[4,5]imidazo[1,2-a]pyrazolo[4,3-e]pyrimidin-4(1H)-one (**12**).* 2.0 M thionyl chloride solution in CH_2Cl_2 (130 μL, 0.26

mmol) was added to a solution of 6-((1*R*,2*R*)-2-hydroxycyclopentylamino)-5-methyl-3-phenylamino-2*H*-pyrazolo[3,4-d]pyrimidin-4(5*H*)-one (30 mg, 0.088 mmol) in a mixture of CH_2Cl_2 (1.0 mL) and THF (1.5 mL) at room temperature. After the completion of the addition, the reaction mixture was stirred at room temperature overnight. The mixture was treated with 28% ammonium hydroxide (50μL) and then evaporated to dryness. The obtained residue was purified by silica-gel column chromatography using a gradient of 0 – 100% ethyl acetate in hexane as eluent to afford the title compound as an off-white solid (26 mg, 91% yield). ^{1}H NMR (500 MHz, DMSO-d_6) δ 7.55 (s, 1H), 7.40 (dd, J = 8.5, 7.4 Hz, 2H), 7.22 (d, J = 7.3 Hz, 2H), 7.18 – 7.13 (m, 1H), 4.76 – 4.62 (m, 2H), 3.35 (s, 3H), 2.23 – 2.16 (m, 1H), 1.99 – 1.91 (m, 1H), 1.87 – 1.78 (m, 1H), 1.75 – 1.66 (m, 2H), 1.59 – 1.51 (m, 1H). MS (ESI) *m/z* 323.2 $[M+H]^+$.

*Step e. (6aR,9aS)-5,6a,7,8,9,9a-Hexahydro-1-(cyclopentylmethyl)-5-methyl-3-phenylamino-cyclopent[4,5]imidazo[1,2-a]pyrazolo[4,3-e]pyrimidin-4(1H)-one (**30**).* A suspension of (iodomethyl)cyclopentane (65 mg, 0.31 mmol), cesium carbonate (101 mg, 0.31 mmol) and (6a*R*,9a*S*)-5,6a,7,8,9,9a-hexahydro-5-methyl-3-(phenylamino)-cyclopent[4,5]imidazo[1,2-*a*]pyrazolo[4,3-*e*]pyrimidin-4(1*H*)-one (50 mg, 0.016 mmol) in butan-2-one (1.2 mL) in a sealed vial was heated in a microwave reactor at 140 °C for 0.5 h. After the solvent was removed under reduced pressure, the residue was purified with a semi-preparative HPLC system using a gradient of 0 – 40% acetonitrile in water containing 0.1% formic acid over 16 min to afford the title compound as a white solid (8.0 mg, 13% yield).^{1}H NMR (500 MHz, $CDCl_3$) δ 7.55 (d, J = 7.7 Hz, 2H), 7.52 (s, 1H), 7.31 (dd, J = 8.6, 7.3 Hz, 1H), 6.99 – 6.90 (m, 1H), 4.93 – 4.78 (m, 2H), 4.07 (dd, J = 13.8, 7.0 Hz, 1H), 3.87 (dd, J = 13.8, 7.8 Hz, 1H), 3.43 (s, 3H), 2.59 – 1.21 (m, 15H). MS (ESI) *m/z* 405.2 $[M+H]^+$. HRMS (ESI) *m/z* calcd for $C_{23}H_{29}N_6O$ $[M+H]^+$: 405.2403; found: 405.2396. HPLC purity: 96.0%; retention time: 18.5 min.

(6a*R*,9a*S*)-5,6a,7,8,9,9a-Hexahydro-5-methyl-3-phenylamino-2-(4-(pyridin-2-yl)benzyl)-cyclopent[4,5]imidazo[1,2-*a*]pyrazolo[4,3-*e*]pyrimidin-4(2*H*)-one (47). To a solution of (6a*R*,9a*S*)-5,6a,7,8,9,9a-hexahydro-5-methyl-3-phenylamino-cyclopent[4,5]imidazo[1,2-*a*]pyrazolo[4,3-

e]pyrimidin-4(1*H*)-one (22 mg, 0.068 mmol) and 2-(4-(bromomethyl)phenyl)pyridine (17 mg, 0.068 mmol) in DMF (2.5 mL) was added potassium carbonate (10 mg, 0.068 mmol). The reaction mixture was stirred at room temperature overnight. After the solvent was removed under reduced pressure, the residue was purified with a semi-preparative HPLC system using a gradient of 0 – 60% acetonitrile in water containing 0.1% formic acid over 16 min to afford the title compound as a white solid (5.0 mg, 15% yield). ^{1}H NMR (400 MHz, $CDCl_3$) δ 8.95 – 8.90 (m, 1H), 8.15 – 8.06 (m, 1H), 7.86 – 7.79 (m, 3H), 7.60 – 7.54 (m, 1H), 7.38 – 7.29 (m, 2H), 7.24 – 7.17 (m, 1H), 7.16 (s, 1H), 7.09 (d, J = 8.4 Hz, 2H), 6.97 (d, J = 7.8 Hz, 2H), 5.17 – 4.91 (m, 4H), 3.50 (s, 3H), 2.45 (dd, J = 14.0, 6.0 Hz, 1H), 2.35 – 2.23 (m, 1H), 2.00 – 1.81 (m, 3H), 1.81 – 1.61 (m, 1H). ^{13}C NMR (126 MHz, $CDCl_3$) δ 159.6, 156.9, 153.0, 149.8, 147.6, 144.0, 140.6, 138.9, 136.8, 136.5, 129.6, 127.8, 127.0, 123.9, 122.3, 120.5, 120.1, 89.6, 69.9, 62.5, 52.9, 35.4, 32.3, 28.5, 23.2. MS (ESI) *m/z* 490.1 $[M+H]^+$. HRMS (ESI) *m/z* calcd for $C_{29}H_{28}N_7O$ $[M+H]^+$: 490.2355; found: 490.2367. HPLC purity: 97.6%; retention time: 9.80 min.

Representative synthetic procedures of pyrazolo-pyrimidinones shown in Scheme 3. (6a*R*,9a*S*)-5-Methyl-3-(phenylamino)-2-(4-(6-fluoropyridin-2-yl)-benzyl)-5,6a,7,8,9,9a-hexahydrocyclopent[4,5]imidazo[1,2-*a*]pyrazolo[4,3-*e*]pyrimidin-4(2*H*)-one phosphate (3). *Step a. 7-(4-Methoxybenzyl)-5-methyl-2H-pyrazolo[3,4-d] pyrimidine-4,6(5H,7H)-dione (**13**).* To a solution of 6-hydrazinyl-1-(4-methoxybenzyl)-3-methylpyrimidine-2,4(1*H*,3*H*)-dione (4.0 g, 14.5 mmol) in DMF (200 mL), $POCl_3$ (16 mL) was added dropwise at 0°C. After the addition was completed, the mixture was warmed up to room temperature and stirred overnight. DMF was removed under reduced pressure and the residue was treated with water (100 mL). The resulting precipitate was filtered, washed with water (2 × 50 mL), and dried under high vacuum to give 7-(4-methoxybenzyl)-5-methyl-2*H*-pyrazolo[3,4-*d*]pyrimidine-4,6(5*H*,7*H*)-dione as an off-white solid (3.7 g, 90% yield). ^{1}H NMR (500 MHz, DMSO-d_6) δ 13.51 (s, 1H), 8.50 (s, 1H), 7.31 (d, J = 8.5 Hz, 2H), 6.86 (d, J = 8.5 Hz, 2H), 5.05 (s, 2H), 3.71 (s, 3H), 3.22 (s, 3H). MS (ESI) *m/z* 287.1 $[M+H]^+$.

*Step b. 2-(4-(6-Fluoropyridin-2-yl)benzyl)-7-(4-methoxybenzyl)-5-methyl-2H-pyrazolo[3,4-d]pyrimidine-4,6(5H,7H)-dione (**14**).* To a solution of 7-(4-methoxybenzyl)-5-methyl-2*H*-pyrazolo[3,4-*d*]pyrimidine-4,6(5*H*,7*H*)-dione (1.0 g, 3.49 mmol) and 2-(4-(bromomethyl)phenyl)-6-fluoropyridine (774 mg, 3.49 mmol) in DMF (10 mL) was added potassium carbonate (483 mg, 3.49 mmol). The reaction mixture was stirred at room temperature overnight. After the solvent was removed under reduced pressure, the residue was purified by silica-gel column chromatography using a gradient of 0 – 100% methylene chloride/methanol (5/1, v/v) in hexane as eluent to afford the title compound as a white solid (1.60 g, 97% yield). ^{1}H NMR (500 MHz, $CDCl_3$) δ 8.03 (d, J = 8.3 Hz, 2H), 7.91 – 7.83 (m, 2H), 7.63 (dd, J = 7.5, 2.3 Hz, 1H), 7.46 (d, J = 8.6 Hz, 2H), 7.37 (d, J = 8.3 Hz, 2H), 6.90 (dd, J = 8.1, 2.9 Hz, 1H), 6.81 (d, J = 8.7 Hz, 2H), 5.35 (s, 2H), 5.13 (s, 2H), 3.76 (s, 3H), 3.36 (s, 3H). MS (ESI) *m/z* 472.2 $[M+H]^+$.

*Step c. 2-(4-(6-Fluoropyridin-2-yl)benzyl)-5-methyl-2H-pyrazolo[3,4-d]pyrimidine-4,6(5H,7H)-dione (**15**).* To a solution of 2-(4-(6-fluoropyridin-2-yl)benzyl)-7-(4-methoxybenzyl)-5-methyl-2H-pyrazolo[3,4-*d*]pyrimidine-4,6(5*H*,7*H*)-dione (800 mg, 1.7 mmol) in methylene chloride (2.0 mL) was added trifluoroacetic acid (3.0 mL), followed by trifluoromethanesulfonic acid (0.45 mL, 5.1 mmol). The reaction mixture was stirred at room temperature overnight. After the solvents were removed under reduced pressure, the residue was treated with water (100 mL), and then adjusted to pH = 8 – 9 with 28% ammonium hydroxide. The resulting precipitate was filtered, washed successively with water (3 × 100 mL), methanol (50 mL) and methyl *tert*-butyl ether (100 mL), and then dried under high vacuum to afford the title compound as a pale yellow solid (547 mg, 92% yield). ^{1}H NMR (500 MHz, DMSO-d_6) δ 11.65 (s, 1H), 8.60 (s, 1H), 8.11 – 8.01 (m, 3H), 7.92 (dd, J = 7.6, 2.5 Hz, 1H), 7.41 (d, J = 8.2 Hz, 2H), 7.14 (dd, J = 8.0, 2.7 Hz, 1H), 5.40 (s, 2H), 3.15 (s, 3H). MS (ESI) *m/z* 352.1 $[M+H]^+$.

*Step d. 2-(4-(6-Fluoropyridin-2-yl)benzyl)-6-((1R,2R)-2-hydroxycyclopentylamino)-5-methyl-2H-pyrazolo[3,4-d]pyrimidin-4(5H)-one (**16**).* To a stirred suspension of 2-(4-(6-fluoropyridin-2-yl)-benzyl)-5-methyl-2H-pyrazolo[3,4-d]pyrimidine-4,6(5*H*,7*H*)-dione (500 mg, 1.42 mmol) in THF was

added BOP (818 mg, 1.85 mmol), followed by DBU (0.85 mL, 5.69 mmol). After the mixture was stirred at room temperature for 25 min, (1*R*,2*R*)-2-aminocyclopentanol hydrochloride (294 mg, 2.14 mmol) was added. The reaction mixture was stirred at room temperature overnight. After the solvent was removed under reduced pressure, the residue was dissolved in methylene chloride (100 mL), washed with saturated $NaHCO_3$ (3 × 100 mL) and 0.10 N HCl (3 × 100 mL) successively. The organic phase was evaporated under reduced pressure and the obtained crude product was purified by silica-gel column chromatography using a gradient of 0 – 5% methanol in methylene chloride as eluent to afford the title as a pale yellow solid (507 mg, 82% yield). ^{1}H NMR (500 MHz, $CDCl_3$) δ 7.99 (d, J = 8.3 Hz, 2H), 7.89 (s, 1H), 7.87 – 7.81 (m, 1H), 7.60 (dd, J = 7.5, 2.3 Hz, 1H), 7.39 (d, J = 8.3 Hz, 2H), 6.87 (dd, J = 8.1, 2.9 Hz, 1H), 5.37 (s, 2H), 4.81 (s, 1H), 4.12 – 4.00 (m, 2H), 3.44 (s, 3H), 2.35 – 2.23 (m, 1H), 2.13 – 2.01 (m, 1H), 1.93 – 1.81 (m, 1H), 1.81 – 1.69 (m, 2H), 1.64 – 1.47 (m, 1H). MS (ESI) *m/z* 435.2 $[M+H]^+$.

*Step e. (6aR,9aS)-5,6a,7,8,9,9a-Hexahydro-5-methyl-2-(4-(6-fluoropyridin-2-yl)-benzyl)-cyclopent[4,5]imidazo[1,2-a]pyrazolo[4,3-e]pyrimidin-4(2H)-one (**17**).* To a solution of 2-(4-(6-fluoropyridin-2-yl)benzyl)-6-((1*R*,2*R*)-2-hydroxycyclopentylamino)-5-methyl-2*H*-pyrazolo[3,4-*d*]pyrimidin-4(5*H*)-one (470 mg, 1.08 mmol) in DMF (7.1 mL) was added thionyl chloride (95 μL, 1.3 mmol) dropwise. The reaction mixture was stirred at room temperature for an hour. After the solvent was removed under reduced pressure, the residue was purified by silica-gel column chromatography using a gradient of 0 – 20% methanol in ethyl acetate as eluent to afford the title compound as an off-white solid (428 mg, 95% yield). ^{1}H NMR (500 MHz, $CDCl_3$) δ 8.03 (d, J = 8.3 Hz, 2H) 7.91 – 7.81 (m, 2H), 7.63 (dd, J = 7.6, 2.4 Hz, 1H), 7.38 (d, J = 8.3 Hz, 2H), 6.90 (dd, J = 8.1, 3.0 Hz, 1H), 5.31 (s, 2H), 4.96 – 4.75 (m, 2H), 3.48 (s, 3H), 2.39 – 2.25 (m, 1H), 2.23 – 2.08 (m, 1H), 1.95 – 1.73 (m, 3H), 1.66 – 1.48 (m, 1H). MS (ESI) *m/z* 417.2 $[M+H]^+$.

*Step f. (6aR,9aS)-5,6a,7,8,9,9a-Hexahydro-3-chloro-5-methyl-2-(4-(6-fluoropyridin-2-yl)-benzyl)-cyclopent[4,5]imidazo[1,2-a]pyrazolo[4,3-e]pyrimidin-4(2H)-one (**18**).* 1.0 M LiHMDS in THF (1.2

mL, 1.2 mmol) was added dropwise to a solution of (6a*R*,9a*S*)-5,6a,7,8,9,9a-hexahydro-5-methyl-2-(4-(6-fluoropyridin-2-yl)benzyl)-cyclopent[4,5]imidazo[1,2-*a*]pyrazolo-[4,3-*e*]pyrimidin-4(2*H*)-one (400 mg, 0.96 mmol) and hexachloroethane (227 mg, 0.96 mmol) in methylene chloride (10 mL) at room temperature. After the reaction mixture was stirred at room temperature for 30 min, additional LiHMDS (1.0 M, 1.8 mL, 1.8 mmol) was added. The mixture was stirred at room temperature for an hour and then quenched with water (100 mL). The aqueous phase was extracted with CH_2Cl_2 twice (2 × 150 mL). The combined organic phase was washed with water (100 mL) and then concentrated under reduced pressure. The obtained residue was purified by silica-gel column chromatography using a gradient of 0 – 100% ethyl acetate in hexane as eluent to afford the title compound as an off-white solid (303 mg, 70% yield). ^{1}H NMR (500 MHz, $CDCl_3$) δ 8.00 (d, J = 7.9 Hz, 2H), 7.93 – 7.77 (m, 1H), 7.60 (dd, J = 7.6, 2.4 Hz, 1H), 7.36 (d, J = 7.8 Hz, 2H), 6.88 (dd, J = 8.1, 2.8 Hz, 1H), 5.34 (s, 2H), 4.88 – 4.72 (m, 2H), 3.43 (s, 3H), 2.25 (dd, J = 12.7, 5.8 Hz, 1H), 2.12 – 2.02 (m, 1H), 1.91 – 1.69 (m, 3H), 1.61 – 1.46 (m, 1H). MS (ESI) *m/z* 451.1 $[M+H]^+$.

*Step g. (6aR,9aS)-5-Methyl-3-(phenylamino)-2-(4-(6-fluoropyridin-2-yl)-benzyl)-5,6a,7,8,9,9a-hexahydrocyclopent[4,5]imidazo[1,2-a]pyrazolo[4,3-e]pyrimidin-4(2H)-one phosphate (**3**).* A suspension of (6a*R*,9a*S*)-5,6a,7,8,9,9a-hexahydro-3-chloro-5-methyl-2-(4-(6-fluoropyridin-2-yl)-benzyl)-cyclopent[4,5]imidazo[1,2-*a*]pyrazolo[4,3-*e*]pyrimidin-4(2*H*)-one (200 mg, 0.44 mmol), aniline (45 μL, 0.49 mmol) and potassium carbonate (123 mg, 0.89 mmol) in *tert*-amyl alcohol (1.2 mL) was degassed with argon, and then xantphos (5.1 mg, 0.0089 mmol) and $Pd_2(dba)_3$ (4.1 mg, 0.0044 mmol) were added. The mixture was degassed with argon again, and then heated at 110 °C for 24 h. Another batch of aniline (45 μL, 0.49 mmol), xantphos (5.1 mg, 0.0089 mmol) and $Pd_2(dba)_3$ (4.1 mg, 0.0044 mmol) was added. The reaction mixture was continued to stir at 110 °C for 20 h. After the solvent was removed under reduced pressure, the residue was dissolved in methylene chloride (100 mL) and washed with water (3 × 50 mL). The organic phase was evaporated to dryness under reduced pressure and the obtained crude product was purified by silica-gel column chromatography using a gradient of 0 – 6% methanol in

ethyl acetate as eluent to give (6a*R*,9a*S*)-5-methyl-3-(phenylamino)-2-(4-(6-fluoropyridin-2-yl)-benzyl)-5,6a,7,8,9,9a-hexahydrocyclopent[4,5]imidazo[1,2-a]pyrazolo[4,3-e]pyrimidin-4(2H)-one as an off-white solid (190 mg, 84% yield). ^{1}H NMR (500 MHz, $CDCl_3$) δ 7.89 (d, J = 8.3 Hz, 2H), 7.86 – 7.79 (m, 1H), 7.58 (dd, J = 7.6, 2.5 Hz, 1H), 7.35 – 7.26 (m, 2H), 7.15 – 7.08 (m, 1H), 7.05 (d, J = 8.3 Hz, 2H), 6.94 (d, J = 7.6 Hz, 2H), 6.90 (br, 1H), 6.86 (dd, J = 8.1, 3.0 Hz, 1H), 4.96 (s, 2H), 4.88 – 4.70 (m, 2H), 3.38 (s, 3H), 2.29 (dd, J = 13.0, 6.1 Hz, 1H), 2.15 – 1.96 (m, 1H), 1.90 – 1.71 (m, 3H), 1.65 – 1.52 (m, 1H). ^{13}C NMR (126 MHz, $CDCl_3$) δ 163.4 (d, J_{CF} = 239 Hz), 159.7, 155.7 (d, J_{CF} = 13 Hz), 153.0, 147.6, 144.1, 141.7 (d, J_{CF} = 8 Hz), 140.5, 137.3, 137.1, 129.6, 127.8, 127.1, 124.1, 120.2, 117.3 (d, J_{CF} = 4 Hz), 107.9 (d, J_{CF} = 38 Hz), 89.5, 69.9, 62.6, 52.8, 35.4, 32.3, 28.5, 23.2. MS (ESI) *m/z* 508.3 $[M+H]^+$.

To a solution of (6a*R*,9a*S*)-5-methyl-3-(phenylamino)-2-(4-(6-fluoropyridin-2-yl)-benzyl)-5,6a,7,8,9,9a-hexahydrocyclopent[4,5]imidazo[1,2-a]pyrazolo[4,3-e]pyrimidin-4(2H)-one (180 mg, 0.36 mmol) in acetonitrile (1.8 mL) was slowly added 85 wt.% H_3PO_4 (41 mg, 0.36 mmol) in acetonitrile (65 μL) at 45 °C. The reaction mixture was stirred at 45 °C for 4 h and then cooled to room temperature. After filtration, the filter cake was washed with acetonitrile (2 × 0.5 mL), and then dried under vacuum to yield the title compound as an off-white solid (208 mg, 97% yield). ^{1}H NMR (500 MHz, DMSO-d_6) δ 8.71 (br, 1H), 8.10 – 8.01 (m, 1H), 7.98 (d, J = 8.3 Hz, 2H), 7.89 (dd, J = 7.6, 2.6 Hz, 1H), 7.23 (d, J = 8.4 Hz, 2H), 7.16 (dd, J = 8.5, 7.3 Hz, 2H), 7.12 (dd, J = 8.1, 2.8 Hz, 1H), 6.86 – 6.81 (m, 1H), 6.80 – 6.76 (m, 2H), 5.34 – 5.19 (m, 2H), 4.77 – 4.64 (m, 1H), 4.62 – 4.53 (m, 1H), 3.12 (s, 3H), 2.11 (dd, J = 13.4, 5.7 Hz, 1H), 1.81 – 1.57 (m, 4H), 1.54 – 1.41 (m, 1H). ^{13}C NMR (126 MHz, $CDCl_3$) δ 162.6 (d, J_{CF} = 236 Hz), 155.9, 154.4 (d, J_{CF} = 13 Hz), 152.4, 146.6, 143.0 (d, J_{CF} = 8 Hz), 142.5, 141.8, 138.1, 136.0, 128.7, 127.5, 126.7, 120.4, 117.7 (d, J_{CF} = 4 Hz), 116.0, 108.1 (d, J_{CF} = 37 Hz), 90.3, 66.3, 62.4, 50.6, 34.2, 31.2, 28.5, 22.5. MS (ESI) *m/z* 508.3 $[M+H]^+$. HRMS (ESI) *m/z* calcd for $C_{29}H_{27}N_7OF$ [M (free base)+H]$^+$: 508.2261; found: 508.2272. HPLC purity: 100.0%; retention time: 13.0 min.

(6a*R*,9a*S*)-5,6a,7,8,9,9a-Hexahydro-2-(4-(6-fluoropyridin-2-yl)-benzyl)-5-methyl-3-propylamino-cyclopent[4,5]imidazo[1,2-*a*]pyrazolo[4,3-*e*]pyrimidin-4(2*H*)-one (51). A suspension of propylamine (0.50 mL, 6.08 mmol) and (6a*R*,9a*S*)-5,6a,7,8,9,9a-hexahydro-3-chloro-5-methyl-2-(4-(6-fluoropyridin-2-yl)-benzyl)-cyclopent[4,5]imidazo[1,2-*a*]pyrazolo[4,3-*e*]pyrimidin-4(2*H*)-one (25 mg, 0.055 mmol) in a sealed vial was heated in a microwave reactor at 150 °C for 30 min. After the solvent was removed under reduced pressure, the residue was purified with a semi-preparative HPLC system using a gradient of 0 – 30% acetonitrile in water containing 0.1% formic acid over 16 min to afford the title compound as a white solid (14 mg, 55% yield). ^{1}H NMR (500 MHz, $CDCl_3$) δ 8.00 (d, J = 8.3 Hz, 2H), 7.90 – 7.81 (m, 1H), 7.61 (dd, J = 7.5, 2.4 Hz, 1H), 7.26 (d, J = 8.1 Hz, 2H), 6.89 (dd, J = 8.1, 2.9 Hz, 1H), 5.30 – 5.17 (m, 2H), 4.96 (t, J = 6.2 Hz, 1H), 4.87 – 4.80 (m, 2H), 3.42 (s, 3H), 3.39 (q, J = 6.6 Hz, 2H), 2.41 – 2.26 (m, 1H), 2.18 – 2.05 (m, 1H), 1.94 – 1.70 (m, 3H), 1.70 – 1.56 (m, 1H), 1.56 – 1.44 (m, 2H), 0.85 (t, J = 7.4 Hz, 3H). ^{13}C NMR (126 MHz, $CDCl_3$) δ 166.8, 163.5 (d, J_{CF} = 239 Hz), 157.9 , 155.5 (d, J_{CF} =14 Hz), 153.3, 149.4, 146.1, 141.9 (d, J_{CF} = 8 Hz), 137.5, 137.3, 127.3 (d, J_{CF} = 78 Hz), 117.4 (d, J_{CF} = 4 Hz), 108.1 (d, J_{CF} = 38 Hz), 86.0, 66.6, 62.9, 52.5, 47.7, 35.0, 32.1, 29.0, 24.1, 23.1, 11.0. MS (ESI) *m/z* 474.2 $[M+H]^+$. HRMS (ESI) *m/z* calcd for $C_{26}H_{29}N_7OF$ $[M+H]^+$: 474.2418; found: 474.2413. HPLC purity: 96.6%; retention time: 11.4 min.

(6a*R*,9a*S*)-5,6a,7,8,9,9a-Hexahydro-2-(4-(6-fluoropyridin-2-yl)-benzyl)-5-methyl-3-(pyridin-4-ylamino)-cyclopent[4,5]imidazo[1,2-*a*]pyrazolo[4,3-*e*]pyrimidin-4(2*H*)-one (58). To a solution of pyridin-4-amine (84 mg, 0.89 mmol) and (6a*R*,9a*S*)-5,6a,7,8,9,9a-hexahydro-3-chloro-5-methyl-2-(4-(6-fluoropyridin-2-yl)benzyl)-cyclopent[4,5]imid-azo[1,2-*a*]pyrazolo[4,3-*e*]pyrimidin-4(2*H*)-one (100 mg, 0.22 mmol) in pyridine (2 mL) was added 1.0 M LiHMDS in THF (0.89 mL, 0.89 mmol) dropwise at room temperature. After the completion of the addition, the reaction mixture was heated in a sealed vial in a microwave reactor at 100 °C for 5 h. The solvents were removed under reduced pressure and the residue was purified with a semi-preparative HPLC system using a gradient of 0 – 15% acetonitrile in water containing 0.1% formic acid over 16 min to give the title compound as an off-white solid (22 mg,

20% yield). ^{1}H NMR (500 MHz, DMSO-d_6) δ 8.16 – 8.09 (m, 2H), 8.08 – 8.02 (m, 1H), 7.98 (d, J = 8.3 Hz, 2H), 7.89 (dd, J = 7.6, 2.5 Hz, 1H), 7.24 (d, J = 8.2 Hz, 2H), 7.12 (dd, J = 8.1, 2.7 Hz, 1H), 6.63 (d, J = 4.4 Hz, 2H), 5.35 – 5.20 (m, 2H), 4.70 – 4.62 (m, 1H), 4.61 – 4.53 (m, 1H), 3.12 (s, 3H), 2.16 – 2.03 (m, 1H), 1.79 – 1.57 (m, 4H), 1.52 – 1.39 (m, 1H). MS (ESI) *m/z* 509.2 $[M+H]^+$. HRMS (ESI) *m/z* calcd for $C_{28}H_{26}N_8OF$ $[M+H]^+$: 509.2214; found: 509.2202. HPLC purity: 96.5%; retention time: 6.20 min.

(6a*R*,9a*S*)-5,6a,7,8,9,9a-Hexahydro-2-(4-(6-fluoropyridin-2-yl)-benzyl)-5-methyl-3-(4-fluorophenoxy)-cyclopent[4,5]imidazo[1,2-*a*]pyrazolo[4,3-*e*]pyrimidin-4(2*H*)-one (73). A mixture of (6a*R*,9a*S*)-5,6a,7,8,9,9a-hexahydro-3-chloro-2-(4-(6-fluoropyridin-2-yl)-benzyl)-5-methyl-cyclopent[4,5]imidazo[1,2-*a*]pyrazolo[4,3-*e*]pyrimidin-4(2*H*)-one (26 mg, 0.058 mmol), 4-fluorophenol (13 mg, 0.12 mmol) and potassium carbonate (24 mg, 0.17 mmol) in dioxane (0.50 mL) in a sealed vial was heated in a microwave reactor at 150 °C for 3 h. After the solvent was removed under reduced pressure, the residue was purified with a semi-preparative HPLC system using a gradient of 0 – 35% acetonitrile in water containing 0.1% formic acid over 16 min to afford the title compound as a white solid (18 mg, 60% yield). ^{1}H NMR (500 MHz, $CDCl_3$) δ 7.96 (d, J = 8.3 Hz, 2H), 7.91 – 7.78 (m, 1H), 7.59 (dd, J = 7.6, 2.4 Hz, 1H), 7.36 (d, J = 8.2 Hz, 2H), 7.06 – 6.92 (m, 4H), 6.88 (dd, J = 8.1, 2.9 Hz, 1H), 5.35 – 5.15 (m, 2H), 4.90 – 4.68 (m, 2H), 3.29 (s, 3H), 2.38 – 2.23 (m, 1H), 2.17 – 1.98 (m, 1H), 1.94 – 1.71 (m, 3H), 1.67 – 1.50 (m, 1H). MS (ESI) *m/z* 527.2 $[M+H]^+$. HRMS (ESI) *m/z* calcd for $C_{29}H_{25}N_6O_2F_2$ $[M+H]^+$: 527.2007; found: 527.2003. HPLC purity: 99.9%; retention time: 16.2 min.

(6a*R*,9a*S*)-5,6a,7,8,9,9a-hexahydro-2-(4-(6-fluoropyridin-2-yl)-benzyl)-5-methyl-3-phenylthio-cyclopent[4,5]imidazo[1,2-*a*]pyrazolo[4,3-*e*]pyrimidin-4(2*H*)-one (74). To a solution of (6a*R*,9a*S*)-5,6a,7,8,9,9a-hexahydro-2-(4-(6-fluoropyridin-2-yl)-benzyl)-5-methyl-cyclopent[4,5]imidazo[1,2-*a*]pyrazolo[4,3-*e*]pyrimidin-4(2*H*)-one (57 mg, 0.14 mmol) and phenyl disulfide (60 mg, 0.27 mmol) in THF (1.0 mL) was added 1.0 M LiHMDS in THF (0.27 mL, 0.27 mmol) dropwise at room temperature. The reaction mixture was stirred at room temperature for an hour and then quenched with water. After the solvent was removed under reduced pressure, the residue was purified with a semi-preparative

HPLC system using a gradient of 0 – 35% acetonitrile in water containing 0.1% formic acid over 16 min to afford the title compound as a pale yellow solid (27 mg, 38% yield). ^{1}H NMR (500 MHz, $CDCl_3$) δ 7.94 (d, J = 8.0 Hz, 2H), 7.89 – 7.80 (m, 1H), 7.59 (dd, J = 7.5, 2.5 Hz, 1H), 7.42 – 7.16 (m, 7H), 6.89 (dd, J = 8.2, 3.0 Hz, 1H), 5.55 (s, 2H), 5.14 – 4.73 (m, 2H), 3.62 (s, 3H), 2.49 – 2.22 (m, 1H), 1.98 – 1.43 (m, 5H). MS (ESI) *m/z* 525.2 $[M+H]^+$. HRMS (ESI) *m/z* calcd for $C_{29}H_{26}N_6OFS$ $[M+H]^+$: 525.1873; found: 525.1866. HPLC purity: 99.6%; retention time: 18.1 min.

(6a*R*,9a*S*)-5,6a,7,8,9,9a-Hexahydro-3-benzyl-2-(4-(6-fluoropyridin-2-yl)-benzyl)-5-methyl-cyclopent[4,5]imidazo[1,2-*a*]pyrazolo[4,3-*e*]pyrimidin-4(2H)-one (75). To a solution of B-benzyl-9-borabicyclo[3.3.1]nonane in hexane (0.50 M, 1.0 mL, 0.50 mmol) was added benzylzinc chloride in THF (0.50 M, 1.0 mL, 0.50 mmol) dropwise at -78 °C. After the addition was completed, the cooling bath was removed and the reaction mixture was stirred at room temperature for 30 min. A solution of (6a*R*,9a*S*)-5,6a,7,8,9,9a-hexahydro-3-chloro-2-(4-(6-fluoropyridin-2-yl)benzyl)-5-methyl-cyclopent[4,5]imidazo[1,2-*a*]pyrazolo[4,3-*e*]pyrimidin-4(2*H*)-one in DMF (1.0 mL, 23 mg, 0.050 mmol) was added, followed by palladium(II) acetate (1.0 mg, 0.0045 mmol) and 2-dicyclohexylphosphino-2',6'-dimethoxybiphenyl (8.0 mg, 0.020 mmol). The reaction mixture was heated in a microwave reactor at 100 °C for 4 h. After the solvents were removed under reduced pressure, the residue was purified with a semi-preparative HPLC system using a gradient of 0 – 35% acetonitrile in water containing 0.1% formic acid over 16 min to afford the title compound as a white solid (15 mg, 57% yield). ^{1}H NMR (500 MHz, $CDCl_3$) δ 7.92 (d, J = 8.3, 2H), 7.89 – 7.78 (m, 1H), 7.58 (dd, J = 7.5, 2.4 Hz, 1H), 7.31 – 7.15 (m, 5H), 7.09 (d, J = 8.3 Hz, 2H), 6.88 (dd, J = 8.0, 2.9 Hz, 1H), 5.17 (s, 2H), 4.89 – 4.66 (m, 2H), 4.40 – 4.22 (m, 2H), 3.45 (s, 3H), 2.27 (dd, J = 12.1, 5.8 Hz, 1H), 2.14 – 1.96 (m, 1H), 1.90 – 1.69 (m, 3H), 1.64 – 1.53 (m, 1H). MS (ESI) *m/z* 507.3 $[M+H]^+$. HRMS (ESI) *m/z* calcd for $C_{30}H_{28}N_6OF$ $[M+H]^+$: 507.2309; found: 507.2296. HPLC purity: 99.5%; retention time: 16.8 min.

In vitro Phosphodiesterase Inhibition Assays. Phosphodiesterases 1A, 1B, 1C, 2A, 3B, 4A, 5A, 7B, 8A, 9A, 10A, and 11A were generated from full-length human recombinant clones. PDE1, PDE6 were

isolated from bovine brain and bovine retina, respectively. PDE assays were performed in a reaction medium containing 10 mM Tris-HCl (pH 7.2), 10 mM $MgCl_2$, 0.1 % BSA, and 45 nM Fl-cGMP or Fl-cAMP, respectively. This level of substrate is significantly lower than K_m values for PDE enzymes and so measured IC_{50} values are essentially K_i values.[26] Immobilized metal affinity fluorescence polarization (IMAP) assays were carried out for 15 min at room temperature and terminated by addition of binding reagent. Reaction mixture for assay of PDE1 activity also contained 30 μM $CaCl_2$ and 10 U/mL calmodulin. The reaction mixture for assay of PDE2 contained 2 μM cGMP. Fluorescent-labeled cGMP (Fl-cGMP) was used as the substrate in the assays for PDE1, PDE1A, PDE1B, PDE1C, PDE5A, PDE6 and PDE9A, while fluorescent-labeled cAMP (Fl-cAMP) was used as the substrate for PDE2A, PDE3B, PDE4A, PDE7B, PDE8A, PDE10A and PDE11A. K_i values were calculated using nonlinear regression software, fitting a four-parameter one-site dose-response model (XLFit; IDBS, Cambridge, MA).

Novel Object Recognition Studies in Rats. Different groups of adult, male Sprague-Dawley rats (200–250 g, N = 7 rats/dose/test substance) were injected acutely via the intraperitoneal route with either vehicle solution or a test substance in the vehicle solution (2 mL/kg volume) at a range of concentrations. Sixty (60) min later they were placed in an open field apparatus containing two identical objects. The treated rats were allowed to explore the open field for a six-minute period, referred to as the T1 training session. The animals were then returned to their home cages. Twenty-four hours later the rats were again placed in the open field apparatus for a second six-minute test session (the T2 test session), then returned to their home cages. During T2 one of the objects present in the open field was identical to that present during T1 (i.e., the familiar object), while the other was replaced by a new object (i.e., the novel object). Objects and their placement into the open field were varied across rats to avoid positional biases. To control for possible odor cues the objects were cleaned with a 10% ethanol solution at the end of each trial and the floor of the open field wiped down to eliminate possible scent/trail markers. During the test phase, the novel object was also wiped down prior to testing so that the objects would all have the same odor. The rats were videotaped during the T1 and T2 period to ensure accuracy and reliability in the scoring of the behavior. The videotapes were subsequently scored by

two impartial observers who were blind to drug conditions for the time (in sec) spent by each animal in physical contact (exploration) with the novel and familiar objects. The mean (with SEM) time (sec) spent by drug treated and vehicle-treated rats with each object was calculated. A two-way analysis of variance (ANOVA) was conducted followed by a post-hoc Dunnett's comparison of each dose level to vehicle. A difference of $p < 0.05$ was considered statistically significant.

Protein Expression and Purification. The catalytic domain of human PDE1B representing amino acid numbers (146-506) (NCBI Reference Sequence: NM_000924) was amplified by PCR and ligated into a SUMO-fusion vector (LifeSensors). In order to improve the diffraction quality, the long loop, amino acids (449-471), was deleted.[16] DNA sequences of the open reading frame regions of the expression vectors were verified using a DNA sequencer, ABI PRISM 3100 Genetic Analyzer (Applied Biosystems). Protein was expressed in *E. coli* strain *BL21*(DE3) (NIPPON GENE). The protein was purified by nickel affinity chromatography using Ni-NTA (QIAGEN), and then further purified by size exclusion chromatography using a Superdex200 (GE healthcare). The SUMO affinity tag was digested by SUMO Protease 1 (LifeSensors). To remove SUMO Protease 1, SUMO and the uncleaved protein, the digested solution was passed through a Ni-NTA column. Final purity was achieved by ion exchange chromatography using a Mono Q column (GE healthcare). The purified protein was concentrated to 10 mg/mL by ultrafiltration and flash-frozen in liquid nitrogen for storage at −80 °C.

Protein Crystallography. The complex of human PDE1B protein with compound **3** was prepared by incubation of human PDE1B with a 3-fold molar excess of compound **3** on ice for a few hours prior to crystallization experiments. Crystals were grown from a reservoir solution containing 0.1 M Tris pH 8.0, 1.75 M ammonium sulfate at 4 °C by the sitting drop vapor diffusion method. Prior to data collection, crystals were immersed in the reservoir solution with addition of 30% glycerol as a cryoprotectant and were flash-frozen in liquid nitrogen. Diffraction data were collected from a single crystal using the CCD detector Quantum 315 (ADSC) at beamline 5.0.3 of the Advanced Light Source (Berkeley, CA) under a 100 K nitrogen cryostream. The data were reduced and scaled with the program HKL2000.[27] The struc-

ture was solved by the molecular replacement method with Molrep[28] of the CCP4 program suites[29] using the PDE1B apo-enzyme structure (PDB code: 1TAZ) as a search model. The structure was refined through an iterative procedure utilizing REFMAC[30] followed by model building using the program COOT.[31] The dictionary files for the ligands were prepared using AFITT (OpenEye Scientific Software). The final models were validated using Molprobity.[32] Crystallographic processing and refinement statistics are summarized in Table S1 of the Supporting Information. All structural figures were generated using PyMOL (Schrödinger) and LIGPLOT.[33]

ASSOCIATED CONTENT

Supporting Information

Synthesis and analytical data of intermediates and final compounds not listed in the Experimental Section; x-ray crystallographic information for crystals of PDE1B/compound **3**; additional figures to show the details of the interactions between PDE1B enzyme and compound **3**

Molecular formula strings

Accession codes

Atom coordinates and structure factors for the complex of PDE1B/compound **3** have been deposited in the Protein Data Bank with accession code 5B25.

AUTHOR INFORMATION

Corresponding Author

*Phone: 646–440–9388. Fax: 646–440–9334. E-mail: pli@intracellulartherapies.com.

Present Addresses

[£] Tianjin Hospital, 406 Jiefang Nanlu, Hexi District, Tianjin, 300211, P. R. China.

[€] J-Star Research, Inc., 3001 Hadley Road, Suites 1 – 4, South Plainfield, New Jersey 07080, USA.

ACKNOLWEDGEMENTS

This work was supported, in part, by funding from the National Institutes of Health (R43 MH067488-01) to Intra-Cellular Therapies, Inc. The authors wish to thank Dr. Sharon Mates and other team members from Intra-Cellular Therapies, Inc. and Takeda Pharmaceutical Company Ltd. for their contributions to this project and thoughtful comments on the manuscript. We thank the staff of the Berkeley Center for Structural Biology (BCSB) who operate ALS beamline 5.0.3. BCSB is supported in part by the National Institutes of Health, National Institute of General Medical Sciences, and the Howard Hughes Medical Institute. The Advanced Light Source is supported by the Director, Office of Science, Office of Basic Energy Sciences, of the U.S. Department of Energy under Contract No. DE-AC02-05CH11231.

ABBREVIATIONS USED

BOP, benzotriazol-1-yloxy tris(dimethylamino) phosphonium hexafluorophosphate; cAMP, cyclic adenosine monophosphate; cGMP, cyclic guanosine monophosphate; CIAS, cognitive impairment associated with schizophrenia; CNS, central nervous system; D1R, dopamine D1 receptors; DBU, 1,8-diazabicyclo[5.4.0]undec-7-ene; HLM, human liver microsomes; IMAP, immobilized metal affinity fluorescence polarization; LiHMDS, lithium bis(trimethyl-silyl)amide; NOR, novel object recognition; $Pd_2(dba)_3$, tris(dibenzylideneacetone)dipalladium; PDE, cyclic nucleotide phosphodiesterase; PMB, para-methoxybenzyl; SAR, structure–activity relationship; TPSA, topological polar surface area.

REFERENCES

(1) Greengard, P. The neurobiology of slow synaptic transmission. *Science* **2001**, *294*, 1024–1030.

(2) (a) Conti, M.; Beavo, J. Biochemistry and physiology of cyclic nucleotide phosphodiesterases: essential components in cyclic nucleotide signaling. *Annu. Rev. Biochem.* **2007**, *76*, 481–511. (b) Bender, A. T.; Beavo, J. A. Cyclic nucleotide phosphodiesterases: molecular regulation to clinical use. *Pharmacol. Rev.* **2006**, *58*, 488–520.

(3) Jeon, Y. H.; Heo, Y.–S.; Kim, C. M.; Hyun, Y.–L.; Lee, T. G.; Ro, S.; Cho, J. M. Phosphodiesterase: overview of protein structures, potential therapeutic applications and recent progress in drug development. *Cell. Mol. Life Sci.* **2005**, *62*, 1198–1220.

(4) Sonnenburg, W. K.; Seger, D.; Beavo, J. A. Molecular cloning of a cDNA encoding the "61-KDa" calmodulin-stimulated cyclic nucleotide phosphodiesterase. Tissue-specific expression of structurally related isoforms. *J. Biol. Chem.* **1993**, *268*, 645–652.

(5) Kakkar, R.; Raju, R. V. S.; Sharma, R. K. Calmodulin-dependent cyclic nucleotide phosphodiesterase (PDE1). *Cell. Mol. Life Sci.* **1999**, *55*, 1164–1186, and the references cited therein.

(6) (a) Sharma, R. K.; Das, S. B.; Lakshmikuttyamma, A.; Selvakumar, P.; Shrivastav, A. Regulation of calmodulin-stimulated cyclic nucleotide phosphodiesterase (PDE1): Review. *Int. J. Mol. Med.* **2006**, *18*, 95−105. (b) Sharma, R. K.; Kalra, J. Characterization of calmodulin dependent cyclic nucleotide phosphodiesterase isozymes. *Biochem. J.* **1994**, *299*, 97–100.

(7) (a) Polli, J. W.; Kincaid, R. L. Molecular cloning of DNA encoding a calmodulin-dependent phosphodiesterase enriched in striatum. *Proc. Natl. Acad. Sci. USA* **1992,** *89*, 11079–11083. (b) Lakics. V.; Karran, E. H.; Boess, F. G. Quantitative comparison of phosphodiesterase mRNA distribution in human brain and peripheral tissues. *Neuropharmacology* **2010**, *59*, 367–374.

(8) (a) Medina, A. E. Therapeutic utility of phosphodiesterase type 1 inhibitors in neurological conditions. *Front. Neurosci.* **2011**, *5:21*, 1–5. (b) Filgueiras, C. C.; Krahe, T. E.; Medina, A. E. Phosphodiesterase type 1 inhibition improves learning in rats exposed to alcohol during the third trimester equivalent of human gestation. *Neurosci. Lett.* **2010**, *473*, 202–207.

(9) Goldman-Rakic, P. S. Circuitry of the frontal association cortex and its relevance to dementia. *Arch. Gerontol. Geriatr.* **1987**, *6*, 299–309.

(10) Lemon, N.; Manahan-Vaughan, D. Dopamine D1/D5 receptors gate the acquisition of novel information through hippocampal long-term potentiation and long-term depression. *J. Neurosci*. **2006**, *26*, 7723–7729.

(11)(a) Castner, S. A.; Williams, G.V.; Goldman-Rakic, P. S. Reversal of antipsychotic-induced working memory deficits by short-term dopamine D1 receptor stimulation. *Science*, **2000**, *287*, 2020–2022. (b) Goldman-Rakic, P. S.; Castner, S. A.; Svensson, T. H.; Siever, L. J.; Williams, G. V. Targeting the dopamine D1 receptor in schizophrenia: insights for cognitive dysfunction. *Psychopharmacology* **2004**, *174*, 3–16.

(12)Tamminga, C. A.; Buchanan, R. W.; Gold, J. M. The role of negative symptoms and cognitive dysfunction in schizophrenia outcome. *Int. Clin. Psychopharmacol.* **1998**, *13*, Suppl. 3, S21–S26.

(13)(a) Manoach, D. S.; Gollub, R. L.; Benson, E. S.; Searl, M. M.; Goff, D. C.; Halpern, E.; Saper, C. B.; Rauch, S. L. Schizophrenic subjects show aberrant fMRI activation of dorsolateral prefrontal cortex and basal ganglia during working memory performance. *Biol. Psychiatry* **2000**, *48*, 99–109. (b) Koch, K.; Wagner, G.; Nenadic, I.; Schachtzabel, C.; Schultz, C.; Roebel, M.; Reichenbach, J. R.; Sauer, H.; Schlösser, R. G. Fronto-striatal hypoactivation during correct information retrieval in patients with schizophrenia: an fMRI study. *Neuroscience* **2008**, *153*, 54–62. (c) Slifstein, M.; van de Giessen, E.; Van Snellenberg, J.; Thompson, J. L.; Narendran, R.; Gil, R.; Hackett, E.; Girgis, R.; Ojeil, N.; Moore, H.; D'Souza, D.; Malison, R. T.; Huang, Y.; Lim, K.; Nabulsi, N.; Carson, R. E.; Lieberman, J. A.; Abi-Dargham, A. Deficits in prefrontal cortical and extrastriatal dopamine release in schizophrenia: a positron emission tomographic functional magnetic resonance imaging study. *JAMA Psychiatry* **2015**, *72*, 316–24.

(14)Kleppisch, T.; Feil, R. cGMP signalling in the mammalian brain: role in synaptic plasticity and behaviour. *Handb. Exp. Pharmacol.* **2009**, *191*, 547–579.

(15)(a) Card, G. L.; England, B. P.; Suzuki, Y.; Fong, D.; Powell, B.; Lee, B.; Luu, C.; Tabrizizad, M.; Gillette, S.; Ibrahim, P. N.; Artis, D. R.; Bollag, G.; Milburn, M. V.; Kim, S. H.; Schlessinger, J.; Zhang, K. Y. Structural basis for the activity of drugs that inhibit phosphodiesterases. *Structure* **2004**, *12*, 2233–2247. (b) Manallack, D. T.; Hughes, R. A.; Thompson, P. E. The next generation of phosphodiesterase inhibitors: structural clues to ligand and substrate selectivity of phosphodiesterases. *J. Med. Chem.* **2005**, *48*, 3449–3462. (c) Maurice, D. H.; Ke, H.; Ahmad, F.;

Wang, Y.; Chung, J.; Manganiello, V. C. Advances in targeting cyclic nucleotide phosphodiesterases. *Nat. Rev. Drug Discovery* **2014**, *13*, 290–314.

(16)Zhang, K. Y. J.; Card, G. L.; Suzuki, Y.; Artis, D. R.; Fong, D.; Gillette, S.; Hsieh, D.; Neiman, J.; West, B. L.; Zhang, C.; Milburn, M. V.; Kim, S.–H.; Schlessinger, J.; Bollag, G. A. Glutamine switch mechanism for nucleotide selectivity by phosphodiesterases. *Mol. Cell* **2004**, *15*, 279–286.

(17) Pandit, J. (Pfizer Inc.) Crystal structure of 3′,5′-cyclic nucleotide phosphodiesterase 1B (PDE1B) and uses thereof. WO 2004/087906 A1, October 14, 2004.

(18)(a) Manabe, H.; Akuta, K.; Sejimo, H.; Kawasaki, H.; Nukui, E.; Ichimura, M.; Kase, H.; Kawakita, T.; Suzuki, F.; Kitamura, S.; Sato, S.; Ohmori, K. Anti-inflammatory and bronchodilator properties of KF19514, a phosphodiesterase 4 and 1 inhibitor. *Eur. J. Pharmacol.* **1997**, *332*, 97–107. (b) Suzuki, H.; Yamamoto, M.; Shimura, S.; Miyamoto, K.; Yamamoto, K.; Sawanishi, H. Synthesis and cyclic AMP phosphodiesterase 4 isoenzyme inhibitory activity of heterocycle condensed purines. *Chem. Pharm. Bull.* **2002**, *50*, 1163–1168. (c) Haning, H.; Niewöhner, U.; Schenke, T.; Lampe, T.; Hillisch, A.; Bischoff, E. Comparison of different heterocyclic scaffolds as substrate analog PDE5 inhibitors. *Bioorg. Med. Chem. Lett.* **2005**, *15*, 3900–3907. (d) Wells, J. N.; Miller, J. R. Methylxanthine inhibitors of phosphodiesterases. *Methods Enzymol.* **1988**, *159*, 489–496. (e) Wells, J. N.; Garst, J. E.; Kramer, G. L. Inhibition of separated forms of cyclic nucleotide phosphodiesterase from pig coronary arteries by 1,3-disubstituted and 1,3,8-trisubstituted xanthines. *J. Med. Chem.* **1981**, *24*, 954–958. (f) Humphrey, J. M.; Yang, E.; Ende, C. W. a.; Arnold, E. P.; Head, J. L.; Jenkinson, S.; Lebel, L. A.; Liras, S.; Pandit, J.; Samas, B.; Vajdos, F.; Simons, S. P.; Evdokimov, A.; Mansour, M.; Menniti, F. S. Small-molecule phosphodiesterase probes: discovery of potent and selective CNS-penetrable quinazoline inhibitors of PDE1. *MedChemComm* **2014**, *5*, 1290–1296. (g) Ahn, H.–S.; Bercovici, A.; Boykow, G.; Bronnenkant, A.; Chackalamannil, S.; Chow, J.; Cleven, R.; Cook, J.; Czarniecki, M.; Domalski, C.; Fawzi, A.; Green, M.; Gündes, A.; Ho, G.; Laudicina, M.; Lindo, N.; Ma, K.; Manna, M.; McKittrick, B.; Mirzai, B.; Nechuta, T.; Neustadt, B.; Puchalski, C.; Pula, K.; Silverman, L.; Smith, E.; Stamford, A.;

Tedesco, R. P.; Tsai, H.; Tulshian, D.; Vaccaro, H.; Watkins, R. W.; Weng, X.; Witkowski, J. T.; Xia, Y.; Zhang, H. Potent tetracyclic guanine inhibitors of PDE1 and PDE5 cyclic guanosine monophosphate phosphodiesterases with oral antihypertensive activity. *J. Med. Chem.* **1997**, *40*, 2196–2210.

(19) Xia, Y.; Chackalamannil, S.; Czarniecki, M.; Tsai, H.; Vaccaro, H.; Cleven, R.; Cook, J.; Fawzi, A; Watkins, R.; Zhang, H. Synthesis and evaluation of polycyclic pyrazolo[3,4-d]pyrimidines as PDE1 and PDE5 cGMP phosphodiesterase inhibitors. *J. Med. Chem.* **1997**, *40*, 4372–4377.

(20)(a) Zhang, X.; Feng, Q.; Cote, R. H. Efficacy and selectivity of phosphodiesterase-targeted drugs in inhibiting photoreceptor phosphodiesterase (PDE6) in retinal photoreceptors. *Invest. Ophthalmol. Vis. Sci.* **2005**, *46*, 3060−3066. (b) Pissarnitski, D. Phosphodiesterase 5 (PDE 5) inhibitors for the treatment of male erectile disorder: attaining selectivity versus PDE6. *Med. Res. Rev.* **2006**, *26*, 369–395.

(21)Bhuyan, P. J.; Borah, H. N.; Sandhu, J. S. Studies on uracils: a facile one-pot synthesis of pyrazolo[3,4-d]pyrimidines. *Tetrahedron Lett.* **2002**, *43*, 895–897, and the references cited therein.

(22)Wan, Z.–K.; Wacharasindhu, S.; Levins, C. G.; Lin, M.; Tabei, K.; Mansour, T. S. The scope and mechanism of phosphonium-mediated S_NAr reactions in heterocyclic amides and ureas. *J. Org. Chem.* **2007**, *72*, 10194–10210.

(23)Arrieta, A.; Aizpurua, J. M.; Palomo, C. *N,N*-Dimethylchlorosulfitemethaniminium chloride ($SOCl_2$–DMF) a versatile dehydrating reagent. *Tetrahedron Lett.* **1984**, *25*, 3365–3368.

(24)Katritzky, A. R.; Hall, C. D.; El-Gendy, B. El-D. M.; Draghici, B. Tautomerism in drug discovery. *J. Comput. Aided Mol. Des.* **2010**, *24*, 475–484.

(25)Floresco, S. B. Prefrontal dopamine and behavioral flexibility: shifting from an "inverted-U" toward a family of functions. *Front Neurosci.* **2013**, *7:62*, 1–12.

(26)(a) Cheng, H. C. The power issue: determination of K_B or K_i from IC_{50}. A closer look at the Cheng-Prusoff equation, the Schild plot and related power equations. *J Pharmacol. Toxicol. Methods* **2001**, *46*, 61–71. (b) Lazareno, S.; Birdsall, N. J. Estimation of antagonist K_b from inhi-

bition curves in functional experiments: alternatives to the Cheng-Prusoff equation. *Trends Pharmacol. Sci.* **1993**, *14*, 237–239.

(27) Otwinowski, Z.; Minor, W. Processing of X-ray diffraction data collected in oscillation mode. In *Macromolecular Crystallography. Part A*; Carter, C. W., Jr., Sweet, R. M., Eds.; Academic Press: San Diego, CA, 1997; Vol. 276, pp 307–326.

(28) Vagin, A.; Teplyakov, A. MOLREP: an automated program for molecular replacement, *J. Appl. Crystallogr.* **1997**, *30*, 1022–1025.

(29) Bailey, S. The CCP4 suite – programs for protein crystallography, *Acta Crystallogr., Sect. D: Biol. Crystallogr.* **1994**, *50*, 760–763.

(30) Murshudov, G. N.; Skubák, P.; Lebedev, A. A.; Pannu, N. S.; Steiner, R. A.; Nicholls, R. A.; Winn, M. D.; Long, F.; Vagin, A. A. REFMAC5 for the refinement of macromolecular crystal structures. *Acta Crystallogr., Sect. D: Biol. Crystallogr.* **2011**, *67*, 355–367.

(31) Emsley, P.; Lohkamp, B.; Scott, W. G.; Cowtan, K. Features and development of coot. *Acta Crystallogr., Sect. D: Biol. Crystallogr.* **2010**, *66*, 486–501.

(32) Chen, V. B.; Arendall, W. B. 3rd; Headd, J. J.; Keedy, D. A.; Immormino, R. M.; Kapral, G. J.; Murray, L.W.; Richardson, J. S.; Richardson, D. C. MolProbity: all-atom structure validation for macromolecular crystallography. *Acta Crystallogr., Sect. D: Biol. Crystallogr.* **2010**, *66*, 12–21.

(33) Wallace, A. C.; Laskowski, R. A.; Thornton, J. M. LIGPLOT: a program to generate schematic diagrams of protein-ligand interactions. *Protein Eng.* **1996**, *8*, 127–134.

Table of Contents graphic

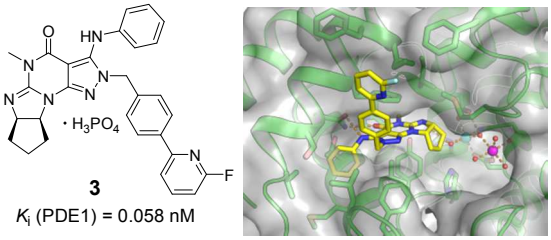

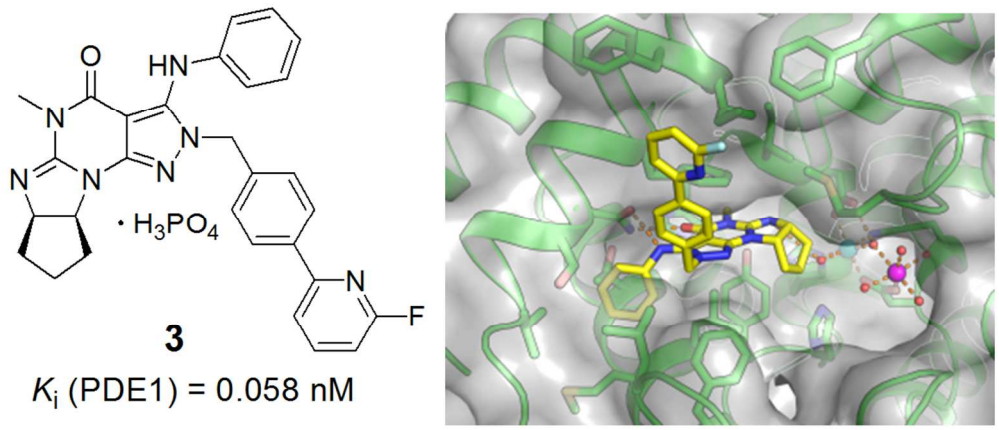

307x131mm (96 x 96 DPI)

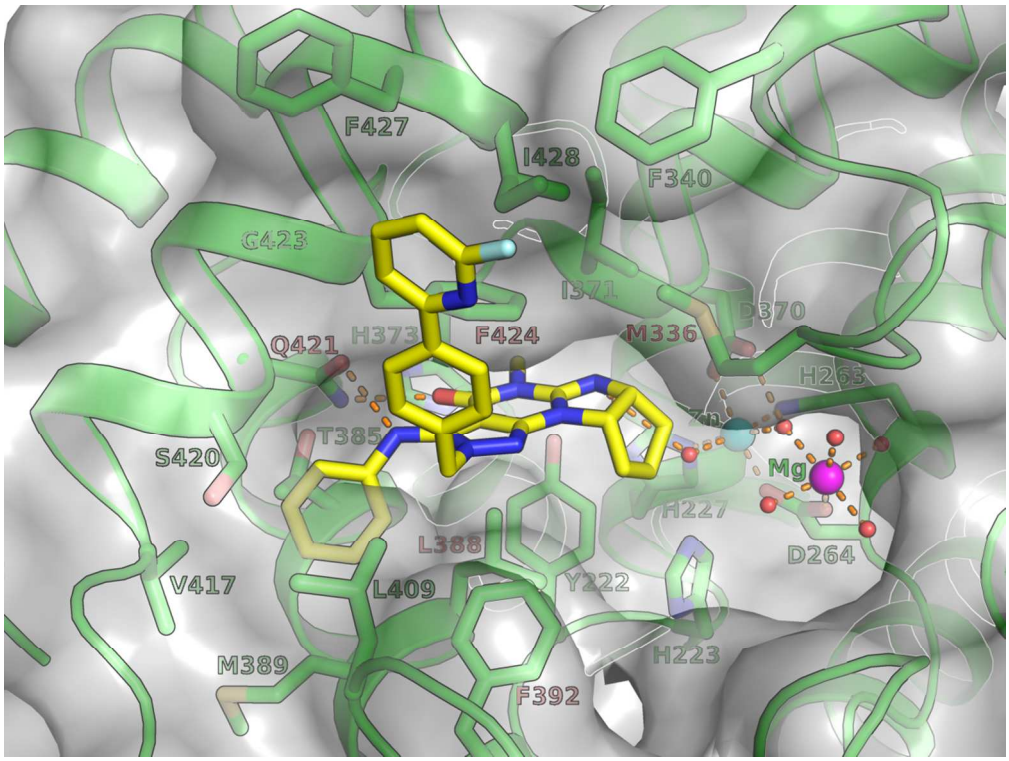

338x254mm (96 x 96 DPI)

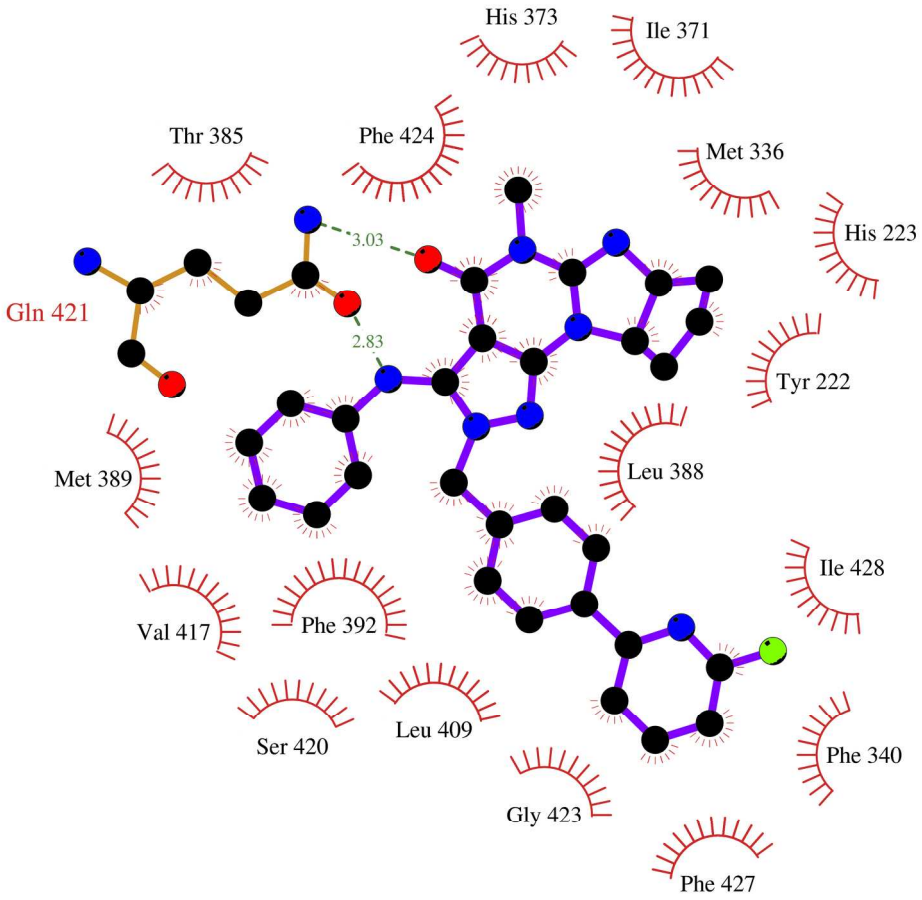

103x98mm (600 x 600 DPI)

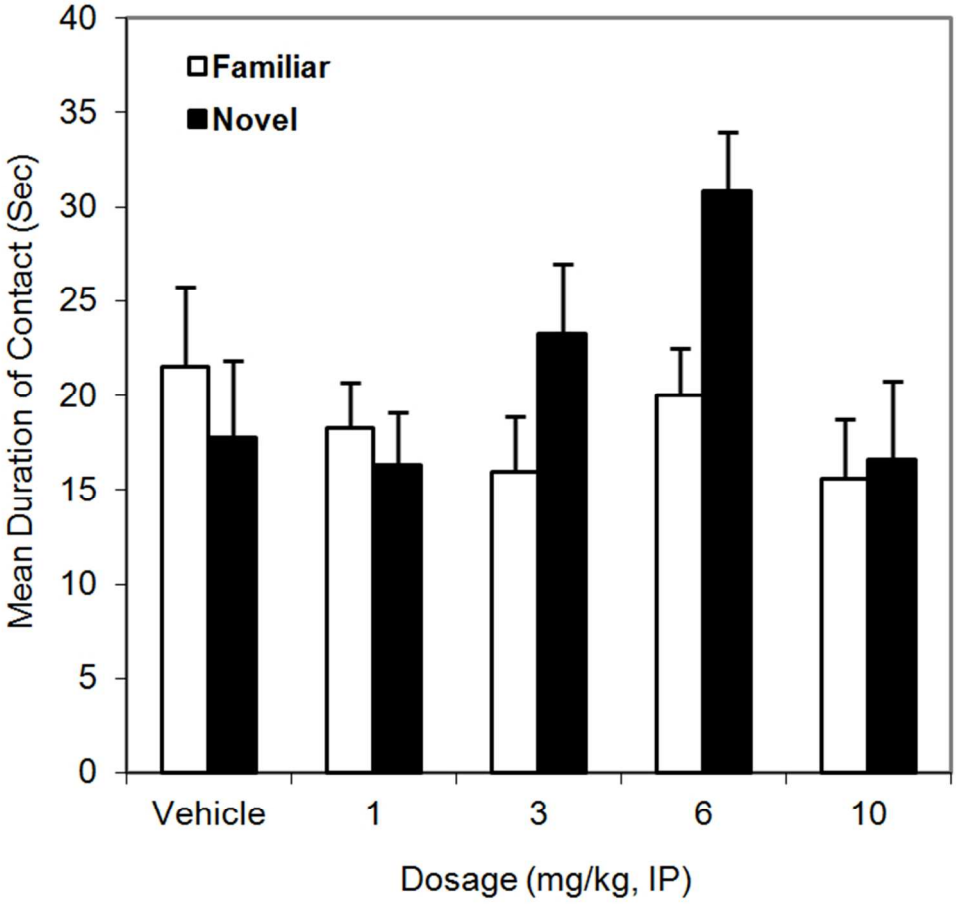

194x180mm (96 x 96 DPI)